Cretaceous Research xxx (xxxx) xxx

Contents lists available at ScienceDirect

Cretaceous Research

journal homepage: www.elsevier.com/locate/CretRes

Soft-tissue preservation in an ichthyosaur from the lower Cretaceous (Barremian - Aptian) of Colombia

Manuel F. Martinez-Motta [a,b], Dirley Cortés [c,d,e,f], Erin E. Maxwell [g], Leslie F. Noè [a], Andrés Alfonso-Rojas [b,d,h], Fredy H. Parra-Ruge [e], Edwin-Alberto Cadena [b,d,i,*]

[a] Departamento de Geociencias, Facultad de Ciencias, Universidad de los Andes, Bogotá D.C., 111221, Colombia
[b] Escuela de Ciencias e Ingeniería, Grupo de Investigación en Paleontología Neotropical Tradicional y Molecular (PaleoNeo), Universidad del Rosario, Bogotá, 111221, Colombia
[c] Department of Biology, McGill University, 1205 Docteur Penfield, Montréal, QC H3A 1B1, Canada
[d] Smithsonian Tropical Research Institute, Box 0843–03092, Balboa, Ancón, Panama
[e] Centro de Investigaciones Paleontológicas, Kilómetro 5.2 vía Santa Sofía, Villa de Leyva, Boyacá, Colombia
[f] Grupo de Investigación Biología para la Conservación, Universidad Pedagógica y Tecnológica de Colombia, Av. Central del Norte 39–115, Tunja, Boyacá, Colombia
[g] Staatliches Museum für Naturkunde Stuttgart, Rosenstein 1, 70191 Stuttgart, Germany
[h] Department of Zoology, and University Museum of Zoology, University of Cambridge, Downing St, Cambridge, CB2 3EJ, UK
[i] Field Museum of Natural History, Chicago, IL, 60605, USA

ARTICLE INFO

Article history:
Received 26 July 2025
Received in revised form
13 December 2025
Accepted in revised form 14 December 2025
Available online xxx

Keywords:
Ichthyosaur
Soft-tissue preservation
Integument
Early Cretaceous
Lower Cretaceous gap
Paja formation biota
Colombia

ABSTRACT

In recent years, global research on soft-tissue preservation in fossils has grown significantly, offering insights into the biology, taphonomy, and diagenesis of extinct organisms. However, studies from low-latitude regions, particularly northern South America, remain limited, and this gap, together with the Lower Cretaceous Gap, restricts our understanding of the processes that enable soft-tissue preservation in these regions. The Paja Formation is a Lower Cretaceous (Hauterivian to Aptian) marine sequence located in central Colombia, notable for its abundant and well-preserved fossils, including vertebrates, invertebrates, and plants. In this study, we analyzed a Barremian-Aptian ichthyosaur from the Paja Formation to investigate soft-tissue preservation. We applied various analytical techniques, including EDTA demineralization, thin-sectioning, transmitted and cross-polarized light microscopy, SEM-EDS, ATR-FTIR spectroscopy, and Raman microspectroscopy. Our findings reveal net-like structures interpreted as fragments of the stratum spinosum layer of the epidermis, composed of N-heterocyclic polymers. We identified laminar and flexible structures defined as the skin-like layer of preserved integumentary tissue, with original proteins transformed into geochemically stable components, including N-heterocyclic polymers and kerogen-like materials. This study reports the first known case of preserved integument in a marine reptile from northern South America. We propose a taphonomic and preservational model based on rapid burial in soft sediment, persistent dysoxic-anoxic regional conditions, microbial biofilm activity, and the formation of early diagenetic carbonate concretions that influenced soft-tissue preservation in this specimen.

1. Introduction

Numerous Lower Cretaceous Konservat-Lagerstätte worldwide have yielded fossils with exceptional soft-tissue preservation (e.g., Martill, 1988; Signore et al., 2005; Lingham-Soliar and Plodowski, 2010; Paik et al., 2010; Martin et al., 2015; Brown et al., 2017; Alfonso-Rojas and Cadena, 2020; Xu et al., 2020). However, most of these are restricted to temperate or subtropical regions (Fig. 1C). The fossil record from low-latitude settings, particularly northern South America, remains limited, especially with respect to soft-tissue preservation and taphonomic processes within the Lower Cretaceous Gap, a critical interval lacking well-preserved marine vertebrate Lagerstätten globally (Gómez-Pérez and Noè, 2017; Noè

* Corresponding author. Escuela de Ciencias e Ingeniería, Grupo de Investigación en Paleontología Neotropical Tradicional y Molecular (PaleoNeo), Universidad del Rosario, Bogotá, 111221, Colombia.
E-mail address: edwin.cadena@urosario.edu.co (E.-A. Cadena).

https://doi.org/10.1016/j.cretres.2025.106305

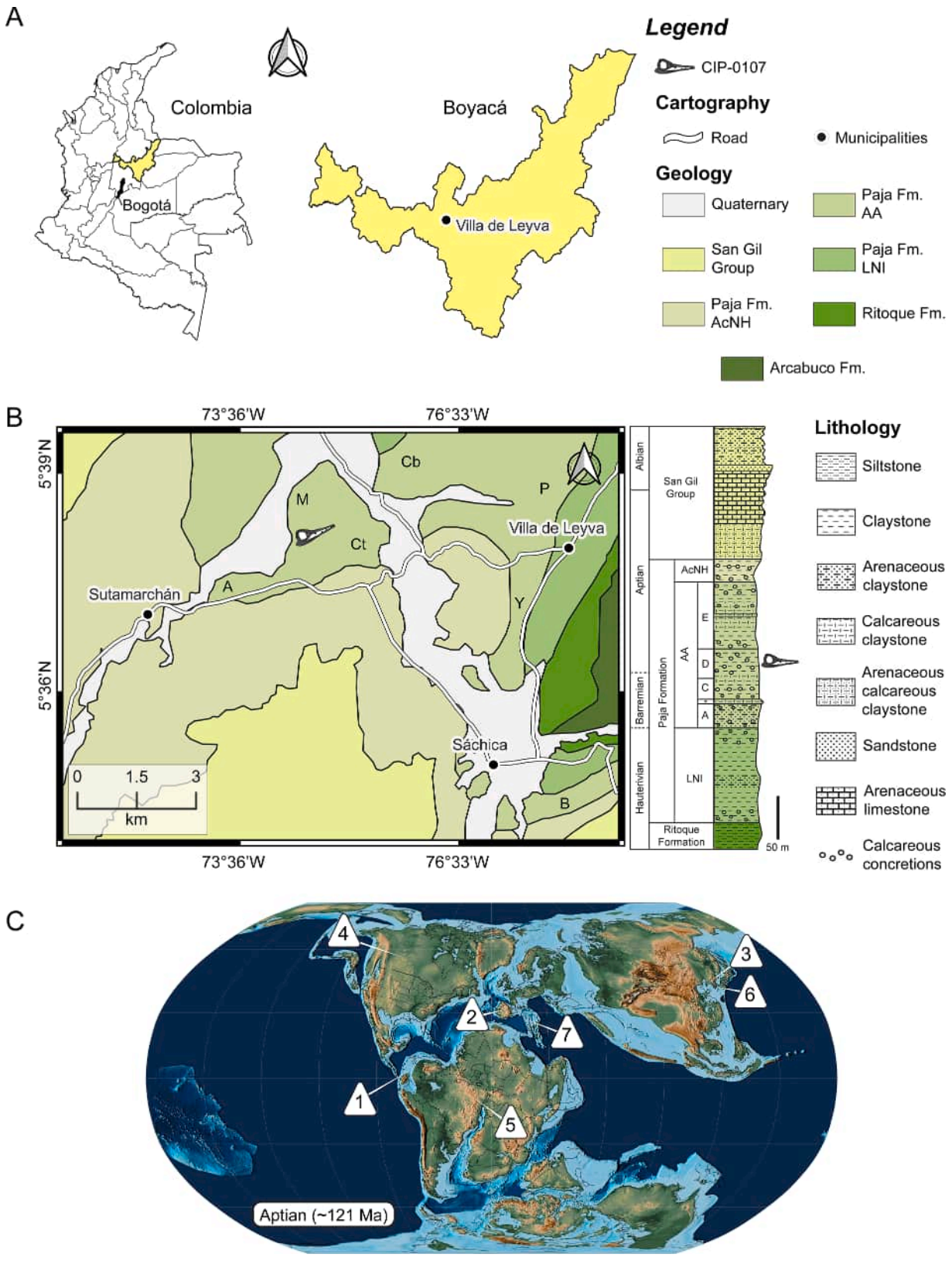

Fig. 1. Locality of ichthyosaur CIP-0107 and other reported exceptionally preserved soft-tissues on vertebrates from the Early Cretaceous. **A**, geographical location of the Alto Ricaurte region, Boyacá Department, within Colombia. **B**, generalized geological and stratigraphic context for the Paja Formation showing the location of CIP-0107 (5°38′N, 73°35′W; complete coordinates are available upon request from the CIP), modified from Etayo-Serna (1965) and Benavides-Cabra et al. (2023). **C**, paleogeographic map during the Aptian (~121 Ma) (from Scotese, 2021), showing localities with exceptionally preserved fossils from the Early Cretaceous: 1, Barremian-Aptian, Paja Fm., Colombia (Alfonso-Rojas and Cadena, 2020; this study); 2, Barremian, Calizas de la Huérgina Fm., Spain (Martin et al., 2015); 3, Barremian-Aptian, Huajiying and Yixian formations (Xu et al., 2020) and Yixian Fm., China (Lingham-Soliar and Plodowski, 2010); 4, Aptian, Clearwater Fm., Canada (Brown et al., 2017); 5, Aptian-Albian, Romulado Fm., Brazil (Martill, 1988); 6, Aptian-Albian, Haman Fm., South Korea (Paik et al.,

& Gómez-Pérez, 2020). Among marine vertebrate fossils worldwide, ichthyosaurs are notable for their exceptional, frequently documented preservation of soft tissues, such as skin (integument), muscles, and possibly internal organs (Eriksson et al., 2022).

Ichthyosaurs with preserved soft-tissue remains have been described from various regions, mainly the Jurassic of Europe, including the Lower to Upper Jurassic of southern England (e.g., Delair, 1966; Martill, 1987a; Martill, 1995; Lingham-Soliar, 1999; Jacobs and Martill, 2020), the Lower and Upper Jurassic of southern Germany (e.g., Bardet and Fernández, 2000; Lingham-Soliar, 2001; Lindgren et al., 2018, 2025; Delsett et al., 2022; De La Garza et al., 2023), and the Lower Jurassic of Luxembourg (Bonnevier-Wallstedt et al., 2024). This exceptional preservation has also been documented in Triassic ichthyosaurs from China and Italy (Motani et al., 1996; Renesto et al., 2020). These studies have provided valuable insights into the anatomy, physiology, and behavior of these ichthyosaurs, while offering a window into the mechanisms of exceptional preservation. The investigation of soft tissues in ichthyosaurs also potentially offers insights into pigmentation, integumentary structure, and environmental adaptations (Eriksson et al., 2022).

The exact nature of these soft-tissue remains has been the subject of considerable debate (Martill, 1993; Schweitzer, 2011; Senter, 2022, and references therein). Even when researchers agree that vertebrate soft tissues are indeed preserved, the interpretation of such remains is often controversial and demands in-depth, multiproxy analyses. For instance, a long-standing discussion involves the fibrous textures described in a small ichthyosaur from the Lower Jurassic of the UK (Delair, 1966), later regarded as fossilized dermal collagen fibers (Lingham-Soliar, 1999), and subsequently reinterpreted as sedimentary features and the result of specimen preparation (Smithwick et al., 2017). These early studies relied exclusively on morphological observations (Delair, 1966; Lingham-Soliar, 1999), and therefore their interpretations lacked sufficient evidence to distinguish soft-tissue remains from other possible origins (Smithwick et al., 2017). However, recent studies have demonstrated how multiproxy analytical approaches can effectively discriminate soft-tissue preservation from sedimentary features (Lindgren et al., 2018, 2025; Marx et al., 2025). These controversies highlight the importance of integrating macroscopic, microstructural, and analytical evidence to interpret fossil soft tissues.

In contrast to well-documented Jurassic sites, Early Cretaceous biotas, particularly those from northern South America remain poorly understood. Recently, however, the Paja Formation in central Colombia has garnered increased scientific attention. A particularly notable region is the Alto Ricaurte Marine Reptile Lagerstätte (Noè and Gómez-Pérez, 2020), situated around the municipalities of Villa de Leyva, Sáchica, and Sutamarchán in the Department of Boyacá (Figs. 1A and 1B). The Paja Formation was also recently included in a list of important Geological Heritage Sites (International Union of Geological Sciences, 2022).

Despite the Paja Formation's rich vertebrate fossil record, its potential for exceptional soft-tissue preservation, a biogenic and taphonomic characteristic of Konservat-Lagerstätten (Kimmig and Schiffbauer, 2024) is only just beginning to be explored and fully understood. Currently documented examples include chemically characterized fossilized turtle eggs (Cadena et al., 2019; Noè and Gómez-Pérez, 2020), potential buccal connective tissue in an ichthyosaur (Cortés et al., 2021), although lacking detailed analysis, and hatchling turtles (Palma-Castro et al., 2023). These finds are typically preserved in early diagenetic concretions, which are likely to enhance soft-tissue preservation (Noè and Gómez-Pérez, 2020; Martin et al., 2021; Dhami et al., 2023). Another example is the 'skin' reported in a fish from the Paja Formation of Zapatoca, Santander (Alfonso-Rojas and Cadena, 2020).

Given this context, the present study aims to identify and characterize potential soft-tissue preservation in an ichthyosaur (CIP-0107) from the Lower Cretaceous Paja Formation of Colombia, housed in the vertebrate collection of the Centro de Investigaciones Paleontológicas (CIP) in Villa de Leyva. We applied advanced analytical techniques to evaluate the presence and composition of preserved soft tissues in CIP-0107. Furthermore, we analyzed the microstructural and geochemical composition to detect ichthyosaurian biomolecular residues and to evaluate the preservation pathway of these tissues. Our study also examined the sedimentological and geochemical context, as well as the depositional environment, which may have contributed to the exceptional preservation of soft tissues in this Early Cretaceous ichthyosaur. These findings thereby enhance our understanding of the mechanisms driving exceptional fossil preservation in Konservat-Lagerstätten, particularly those located in low-latitude settings such as the Cretaceous Paja Formation in the Alto Ricaurte region of South America.

Institutional Abbreviations: **CIP,** Centro de Investigaciones Paleontológicas, Villa de Leyva, Boyacá, Colombia; **InClay**, InClay S.A.S Geología Especializada, Bogotá, Colombia; **MicroCore**, Microscopy Core Facility, Universidad de los Andes, Bogotá, Colombia.

2. Geological background and fossil assemblage

The Paja Formation of central Colombia is a well-exposed Lower Cretaceous (Hauterivian to Aptian) sedimentary sequence, with an estimated thickness of 900–940 m (Etayo-Serna, 1968, 1979; Patarroyo, 2020). The Paja Formation is divided into three members, in ascending order: Lutitas Negras Inferiores, Arcillolitas Abigarradas, and Arcillolitas con Nódulos Huecos (Etayo-Serna, 1968, 1979; Benavides-Cabra et al., 2023) (Fig. 1B). The depositional environment is interpreted as part of an epicontinental sea lying over an extensional back-arc basin, resulting in the deposition of finely laminated mudrocks, particularly shales, alongside claystones, argillaceous limestones, fine-grained sandstones, and incorporating abundant calcareous concretions (Etayo-Serna, 1968, 1979; Montoya-Arenas and Etayo-Serna, 2019; Noè and Gómez-Pérez, 2020).

Most of the fossil vertebrates from the Alto Ricaurte assemblage of the Paja Formation have been recovered from the Arcillolitas Abigarradas Member, which is constrained to the Barremian-Aptian based on detailed lithostratigraphic and biostratigraphic work in the Villa de Leyva region (Benavides-Cabra et al., 2023). Fossil finds include ichthyosaurs (Páramo-Fonseca, 1997; Maxwell et al., 2016, 2019; Cortés and Páramo-Fonseca, 2018; Cortés et al., 2021; Páramo-Fonseca et al., 2021, 2024), pliosaurids (Hampe, 1992; Páramo-Fonseca et al., 2016, 2018, 2019a, 2023; Gómez-Pérez and Noè, 2017; Noè and Gómez-Pérez, 2022; Benavides-Cabra et al., 2025a), elasmosaurid plesiosaurs (Welles, 1962; Páramo-Fonseca et al., 2019b), turtles (Cadena, 2015; Cadena and Parham, 2015; Cadena et al., 2019; Palma-Castro et al., 2023), fishes (Schultze and Stöhr, 1996; Carrillo-Briceño et al., 2019; Noè and Gómez-Pérez, 2020; Benavides-Cabra et al., 2025b), a crocodylomorph (Cortés et al., 2019), dinosaur remains and footprints

2010); 7, Albian, Pietraroja Plattenkalk, Italy (Signore et al., 2005). **Abbreviations**: **A**, Loma La Asomada; **AA**, Arcillolitas Abigarradas; **AcNH**, Arcillolitas con Nódulos Huecos; **B**, Loma Blanca; **Cb**, Loma La Cabrera; **Ct**, Loma La Catalina; **Fm.**, Formation; **LNI**, Lutitas Negras Inferiores; **M**, Loma Monsalve; **Ma**, Millions of years ago; **P**, Loma Pedro Luis; **Y**, Loma La Yesera.

(Carballido et al., 2015; Cortés et al., 2023), abundant invertebrates (Etayo-Serna, 1979; Luque et al., 2020; Patarroyo, 2020), and plants (Palma-Castro, 2024).

3. Material and methods

3.1. Fossil ichthyosaur

The ichthyosaur, cataloged as CIP-0107, was discovered by F.H. Parra-Ruge during a field expedition organized by the CIP in 2018. Excavation efforts were led by F.H. Parra-Ruge, D. Cortés, E.E. Maxwell, J. Pardo-Pérez, M.L. Parra-Ruge, J.D.D. Parra-Ruge, and I.S. Lorentz. CIP-0107 was recovered from the Barremian-Aptian Arcillolitas Abigarradas Member of the Paja Formation between Loma Monsalve and Loma La Catalina, Villa de Leyva (Boyacá, Colombia) (Fig. 1B). During preparation, a waxy texture was noted in the posterior skull region, covering some bones. E.E. Maxwell and D. Cortés suspected this to be preserved soft tissue and consulted E.A. Cadena regarding further analysis. The specimen was mechanically prepared by F.H. Parra-Ruge and Y.C. Parra-Lamus, with minimal intervention in regions suspected to preserve soft-tissue remains. No chemical treatments or consolidants were applied to these delicate areas. The specimen has subsequently been stored under controlled conditions, including dry and dark cabinets, and in isolation from other specimens in the collection to ensure the conservation of its integrity prior to analysis.

CIP-0107 represents a brachypterygiid ichthyosaur with a presacral length of 185 cm and a total preserved length of 217 cm, and is preserved in several calcareous concretions (see Fig. 2A; preserved elements shaded in green-gray). The skull and presacral vertebral column are preserved in a single elongate concretion, although there are several cracks, most notably in the region between the posterior skull and anterior vertebral column/pectoral girdle, indicating minimal surface weathering prior to collection. Two smaller concretions at the posterior of the ichthyosaur preserve the caudal vertebral centra. A comprehensive anatomical and osteological description is currently underway by D. Cortés and E.E. Maxwell. Based on initial examination, the specimen has been preliminarily identified as *Muiscasaurus* sp., and it might correspond to *Muiscasaurus catheti* Maxwell et al., (2016), due to the slender rostrum and narial shape (Maxwell et al., 2016). CIP-0107 differs anatomically from the Paja Formation ichthyosaur *Kyhytysuka sachicarum* Páramo-Fonseca, (1997); Cortés et al., (2021), which exhibits a considerably more robust jaw, differentiated teeth, and a broader postorbital region (Páramo-Fonseca, 1997; Cortés et al., 2021). CIP-0107 also differs from the recently described '*Platypterygius' elsuntuoso* Páramo-Fonseca et al., (2024), which exhibits unique features of the basioccipital, quadrate, and tooth root morphology (Páramo-Fonseca et al., 2024).

3.2. Sampling for soft tissue analyses

Samples (each 1 cm^3–3 cm^3) showing preservation of soft tissue were collected from different areas of the postorbital region of the right lateral side of the skull using a Dremel rotary tool equipped with a fine, pointed bit. This allowed precise extraction of areas containing soft-tissue preservation while minimizing contamination from the surrounding matrix. Sample CIP-0107-A derives from the posterior cranial region interpreted as the exoccipital region, whereas samples B, C, and D were taken from adjacent areas interpreted as part of the supratemporal region (Figs. 2B and 2C). These samples therefore represent soft-tissue remains directly associated with cranial elements of the specimen, rather than postcranial material. To facilitate identification and tracking, samples were labeled with an alphabetical suffix appended to the specimen reference code, ensuring systematic documentation throughout the analysis (Fig. 2D). Strict handling protocols were followed to minimize contamination at each stage including the use of nitrile gloves and face masks, cleaning work surfaces and tools with 70 % ethanol, wrapping samples in sterilized aluminum foil, and storing them in clean plastic bags with silica gel capsules to minimize humidity during transport from the CIP to the Paleontological Laboratories of the Universidad del Rosario and Universidad de los Andes. Additionally, a fragment of the rock matrix from the concretion, and lacking soft tissue preservation, was collected as a control sample.

The samples underwent detailed analysis, including high-resolution photography using a Nikon Eclipse SMZ1270 stereomicroscope to document any soft-tissue remains and guide appropriate treatment. The analytical protocols adhered are those outlined in Schweitzer et al. (2013), Alfonso-Rojas and Cadena (2020), and references therein.

3.3. Bone demineralization

A fraction of samples of approximately 5 mm^3 with a high potential for soft-tissue preservation were taken from CIP-0107-A, and each treated with disodium ethylenediaminetetraacetic acid (EDTA) (0.5M, pH 8.0) for about ten days. To prevent contamination, the treatment was conducted in sterile glass beakers covered with paraffin paper lips in an isolated part of the laboratory (Figs. 3A and 3B). Subsequently, a sample of the supernatant from each treatment was mounted on clean glass slides for observation under transmitted and polarized light microscopy. The remaining sample was returned to fresh EDTA for an additional five days to three weeks until fully demineralized. A sample of the supernatant was centrifuged at 3000 RPM for 2 min in a 1.5 ml Eppendorf tube to concentrate any soft tissue remnants. After removing the supernatant, 1.5 ml of E-pure water was added, and the sample was centrifuged again. This process was repeated three times with a gentle vortex to fully remove the EDTA both from the supernatant and several laminar and flexible structures obtained from the demineralization process defined here as the skin-like layer. After the final centrifuge, the precipitate containing the soft tissue was resuspended in a small volume of E-pure water to preserve it for further analysis. This protocol is outlined in Cadena (2020), and references therein.

3.4. Thin section preparation

A portion of CIP-0107-A (corresponding to the exoccipital region) without the demineralization treatments was embedded in epoxy resin, cut transversely through the soft tissue, and polished using a Struers Accutom-100 precision cutter and polisher at the Geological Sample Preparation Laboratory of the Universidad de los Andes to produce a standard thin section (Fig. 4A) with a thickness of 30 μm following the protocols outlined in Rossi et al. (2024), and Yang et al. (2024).

3.5. Transmitted and polarized light microscopy

The EDTA supernatant from the treatment in fractions of CIP-0107-A was mounted onto clean glass slides, and potential soft-tissue structures were photographed using transmitted and polarized light on a Leica DM750P microscope at the Paleontological Laboratory of the Universidad del Rosario. Additionally, the CIP-0107-A thin section was examined under the same microscope setting to document comparable structures in situ. The protocols followed those of Schweitzer et al. (2019), Cadena (2020), and Alfonso-Rojas and Cadena (2020).

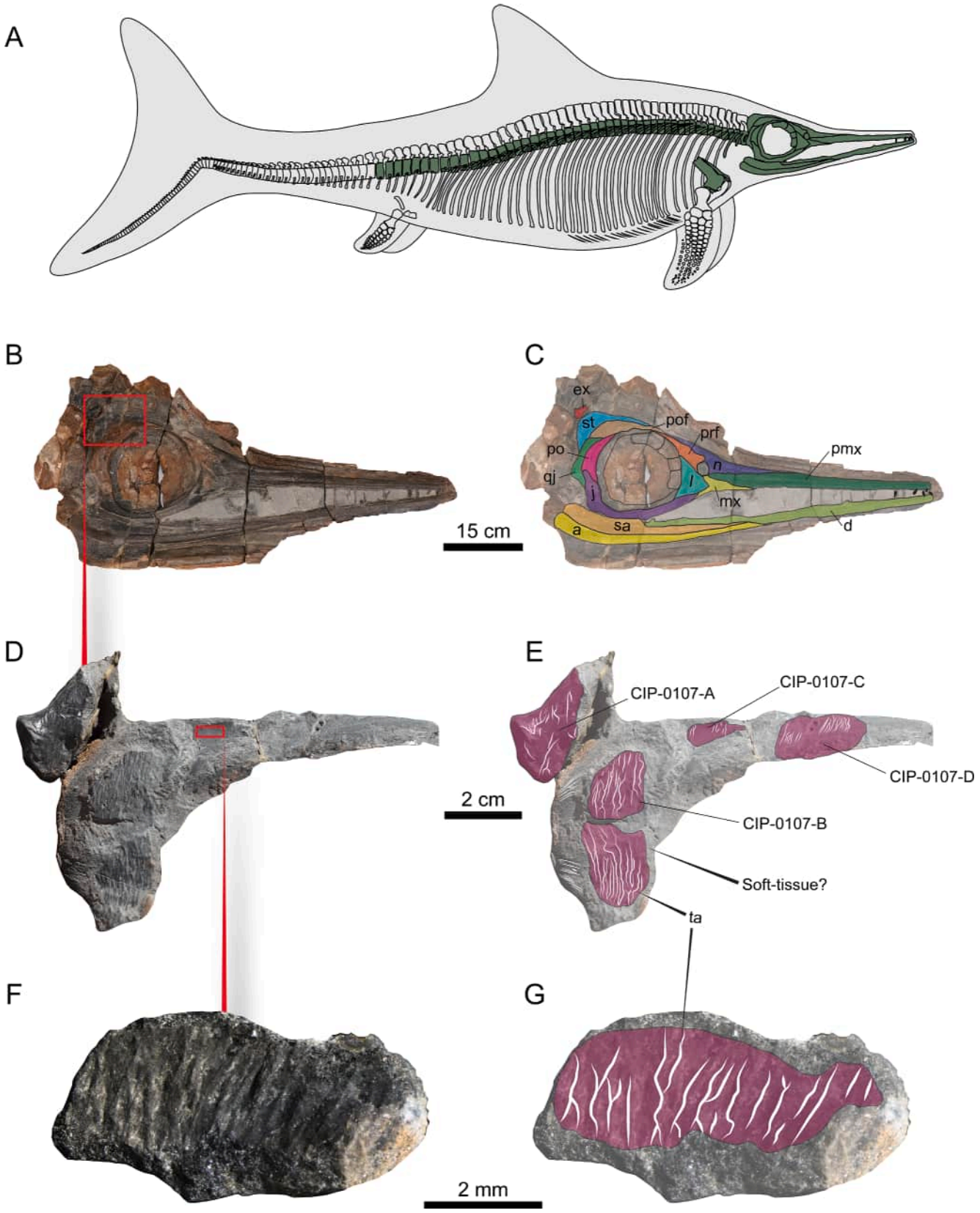

Fig. 2. Ichthyosaur CIP-0107 and the areas of soft-tissue preservation. **A**, generalized body plan of an ichthyosaur highlighting the preserved elements of CIP-0107 (shaded in green-gray). **B**, **C**, skull and generalized osteological interpretation of the right lateral view of the skull of CIP-0107. **D**, **E**, close-up and interpretation of the region with preservation of soft tissue. Sample locations based on alphabetical suffixes are indicated in (E). **F**, **G**, close-up and interpretation of one region with soft-tissue preservation (CIP-0107-C), highlighting tissue alignment. **Abbreviations**: **a**, angular; **d**, dentary; **ex**, exoccipital; **j**, jugal; **l**, lacrimal; **mx**, maxilla; **n**, nasal; **po**, postorbital; **pmx**, premaxilla; **prf**, prefrontal; **pof**, postfrontal; **qj**, quadratojugal; **sa**, surangular; **st**, supratemporal; **ta**, tissue alignment or striations.

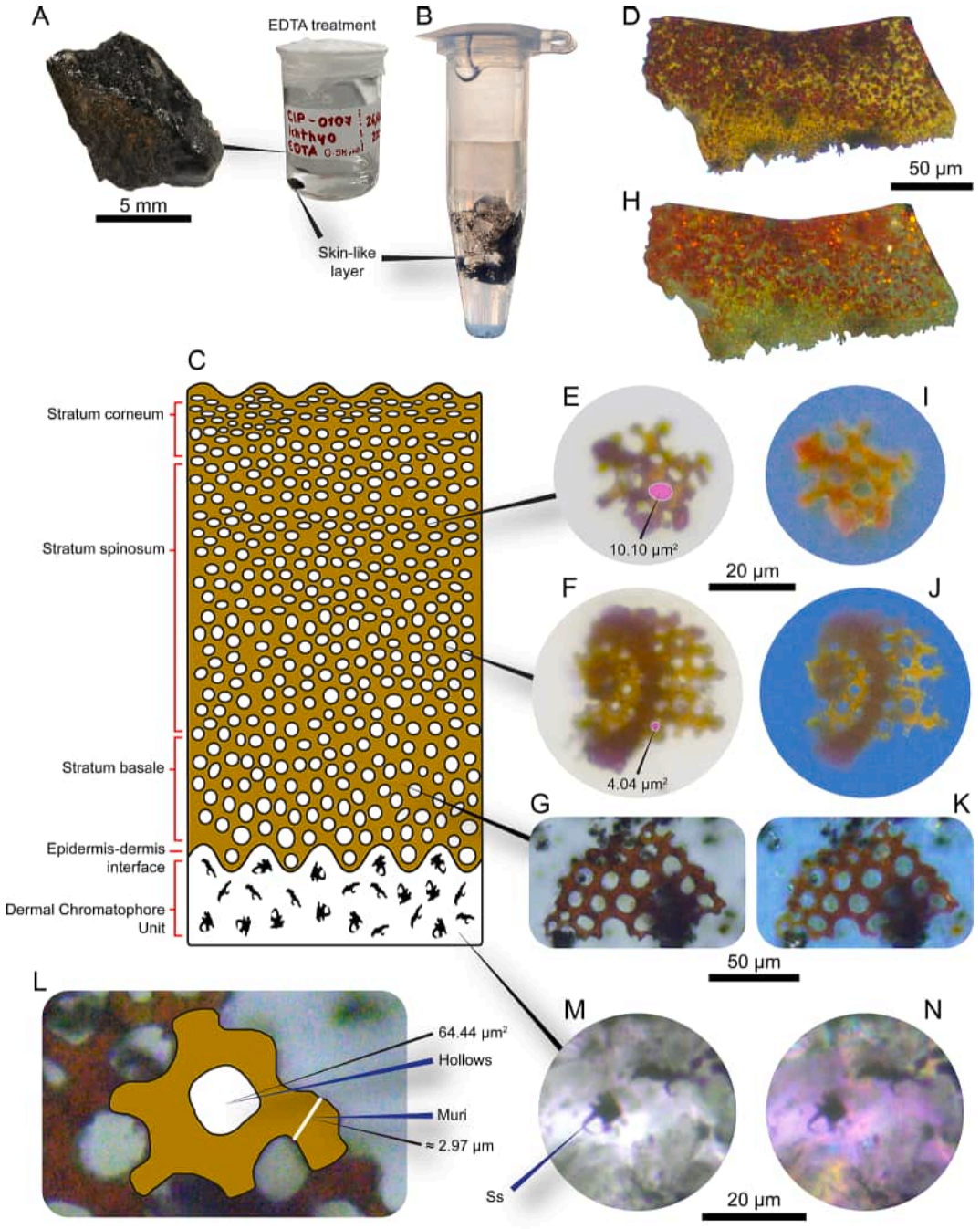

Fig. 3. Soft-tissue remains from CIP-0107 after bone demineralization. **A**, portion of CIP-0107-A before EDTA treatment. **B**, same sample after ~20 days of demineralization, showing the recovery of a flexible, laminar structure identified as a fragment of the skin-like layer. **C**, interpretative diagram of the epidermis-dermis interface of CIP-0107, highlighting morphological subdivisions including the stratum corneum, stratum spinosum, and stratum basale, along with the dermal chromatophore unit. Possible regions of origin for the soft-tissue remains are indicated. **D-G**, photographs under transmitted light microscopy of soft-tissue remains showing net-like structures, with their hollows highlighted in pink, and their corresponding measurements. **H-K**, photographs under cross-polarized light microscopy of soft-tissue remains showing net-like structures. **L**, close-up of (G) showing an interpretation of a net-like structure and their measurements. **M-N**, approximately star-shaped structure embedded in the mineralized integumentary component (mic) in transmitted and cross-polarized light with a Lambda (λ) filter. **Abbreviation**: **EDTA**, disodium ethylenediaminetetraacetic acid; **Ss**, star-shaped structure.

The soft-tissue remains were identified based on their morphology and optical properties through the presence or absence of birefringence under polarized light microscopy. Some remains exhibited a fibrous net-like structure, which was captured in high-resolution images using the Leica LAS-X system software. These images were processed into composite (all-in-focus) images using Helicon Focus software (version 8.0) (Cremona, 2014).

High-resolution images of the net-like structures were analyzed using ImageJ (version 1.52a) (Schroeder et al., 2021). Measurement tools in ImageJ were used to quantify the linear dimensions and areas of the organic material. The averages and

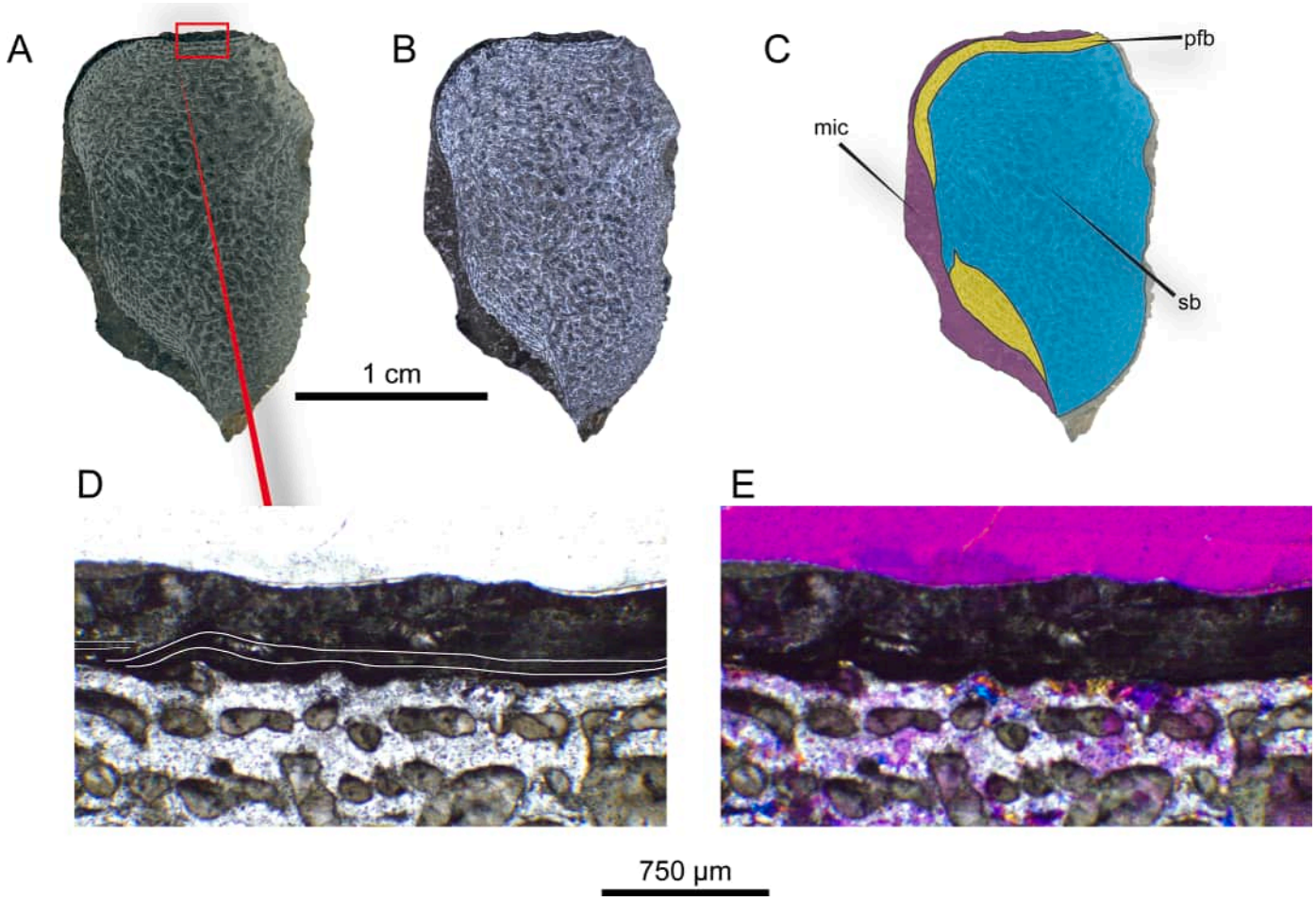

Fig. 4. Thin section of CIP-0107-A under transmitted and cross-polarized light microscopy. **A-B**, complete thin section of CIP-0107-A under transmitted and polarized light respectively. **C**, interpretation of the thin section showing the presence of trabecular bone (spongy bone) in blue, characterized by a crystallization in the porous structure; parallel-fibered bone in yellow, indicative of preserved microstructural details consistent with bone tissue; and mineralized integumentary component (mic) in purple, distinguished by its laminated texture, anatomical position adjacent to the bone, and the presence of internal features suggestive of tissue-level organization. **D-E**, close-up of the transition zone between parallel-fibered bone and mineralized integumentary component, in transmitted and polarized light with a Lambda (λ) filter. **Abbreviations**: **mic**, mineralized integumentary component; **pfb**, parallel-fibered bone; **sb**, spongy bone.

standard deviations were calculated to assess the central tendency and variability of the measurements.

3.6. Scanning electron microscopy coupled with energy dispersive spectroscopy (SEM-EDS)

A drop of the suspended soft-tissue structures was mounted in E-Pure water, along with a fragment of the skin-like layer (~5 mm) extracted from the EDTA demineralization process performed on fractions of CIP-0107-A (section 3.3). These structures were mounted onto a sterile carbon SEM stub and dried at room temperature in a closed SEM-stub box to prevent contamination. Portions of CIP-0107-A, B, C, and D (~5 mm^2 each) were also mounted using sterile tweezers onto carbon stubs and stored in a SEM-stub box until analysis (Figs. 5A and 6F).

The mounted samples were analyzed at MicroCore, using a Tescan Vega SEM-EDS system without a conductive coating. Imaging and elemental composition mapping were conducted at voltages ranging from 10 to 20 kV in low-vacuum conditions. A second analysis was conducted at InClay following the same SEM-EDS setup to ensure consistency across analytical facilities. This comparative approach followed protocols in Cleland et al. (2015), Schweitzer et al. (2019), Alfonso-Rojas and Cadena (2020), and Cadena (2020).

3.7. Fourier transform infrared spectroscopy (FTIR)

Small fractions (~2 mm^2 each) of CIP-0107-A, including samples with soft-tissue preservation untreated, rock matrix (control), and a fragment of the skin-like layer resulting from EDTA treatment performed on fractions of CIP-0107-A, were analyzed using an IRTracer-100 spectrometer at the Laboratorio de Análisis 1 in the Chemistry Department, Universidad de los Andes. The untreated samples were macerated into a fine powder using a sterilized agate mortar, whereas the skin-like layer after being washed with E-pure water was left to dry for about 3 days. To ensure accurate data with reduced noise, the crystal and sample holder of the spectrometer were cleaned with isopropyl alcohol, and the spectrometer was standardized with an "air" measurement to minimize interference from ambient carbon dioxide. The powdered samples were applied to an ATR crystal for mid-infrared range analysis (4,000–400 cm^{-1}), with each measurement repeated twice per sample to ensure consistency. This process followed guidelines established by Lee et al. (2017), Schweitzer et al. (2019), and Alfonso-Rojas and Cadena (2020).

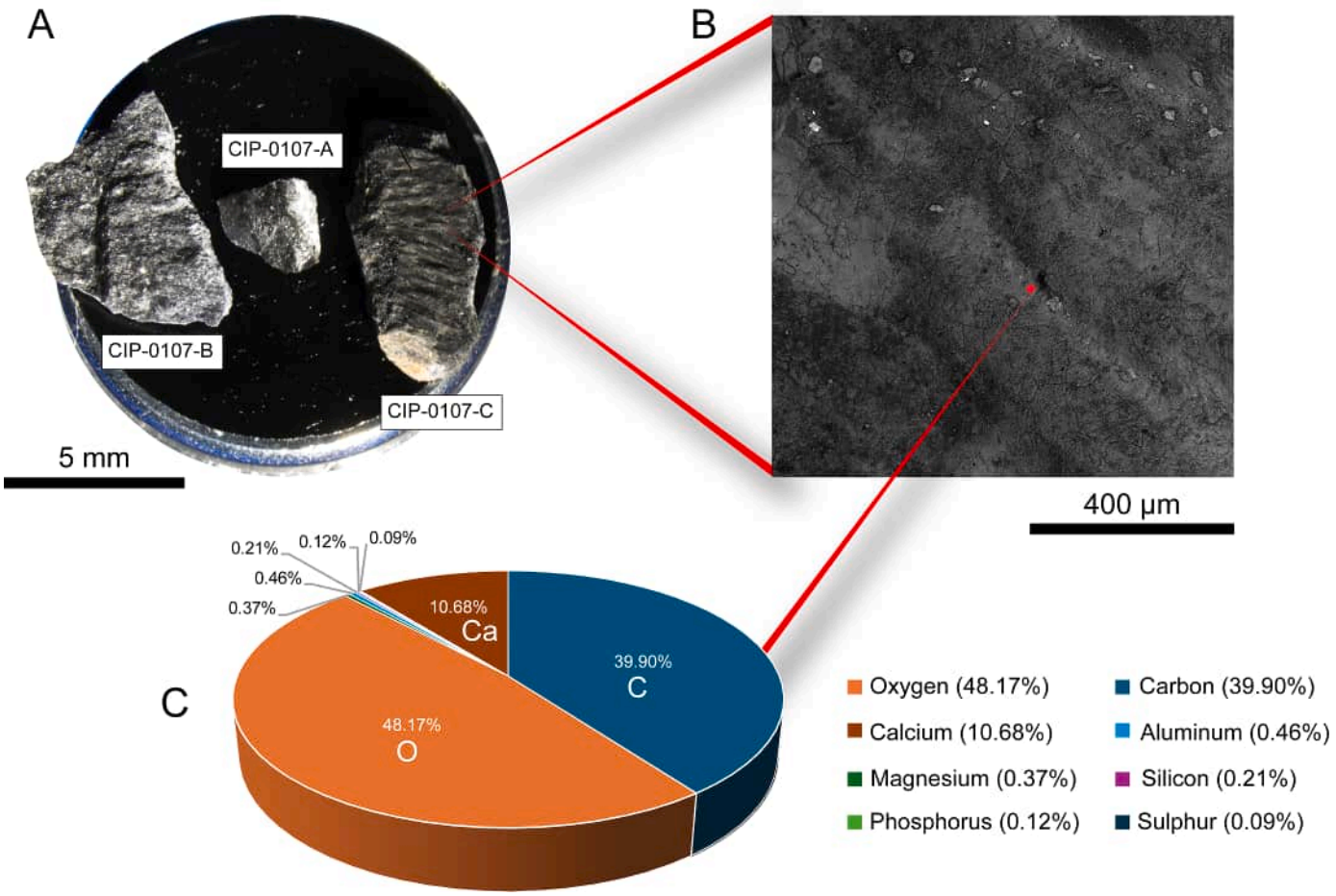

Fig. 5. SEM-EDS analysis and general elemental composition of uncoated fragments of CIP-0107-C. **A**, samples A, B, and C mounted on the SEM-stub. **B**, backscattered electron (BSE) image acquired at 302x magnification and 10 keV of CIP-0107-C. **C**, point elemental analysis marked in (B), revealing a dominance of O, C, and Ca (Atomic %).

3.8. Raman microspectroscopy

A fragment of the skin-like layer obtained from the EDTA demineralization of fractions of CIP-0107-A, after being washed with E-pure water, was analyzed using a Horiba Scientific XploRA confocal Raman microscope at the Laboratorio de Análisis 1 in the Chemistry Department, Universidad de los Andes. The analysis was performed with a 532 nm excitation laser, a 1200 gr/mm diffraction grating, and a 100 × objective lens. The confocal hole and slit width were set to 300 µm and 100 µm, respectively. Spectra were acquired with an integration time of 5 s and 15 accumulations per point, with laser power adjusted between 10 and 25% to avoid sample degradation. The spectral acquisition targeted visually distinct regions of the skin-like layer, including black and brown-stained structures, and a translucent area. No baseline correction or fluorescence filtering was applied to the raw spectra. These protocols followed methodological standards established by Wiemann et al. (2018), Wiemann and Briggs (2022), and references therein.

4. Results

4.1. Macroscopic description of CIP-0107 and potential soft-tissue preservation

The ichthyosaur CIP-0107 consists of an incomplete, three-dimensionally preserved skull that is laterally compressed and observable in right lateral view (Figs. 2B and 2C). The presence of the effects of compression, as a result of fossil diagenesis, has not significantly disrupted the overall anatomical surface of the skull and rostrum in contact with the sediment. However, on the surface of the skull that was in contact with the water column, disarticulation is more pronounced, with braincase elements scattered around the posterior skull, the left parietal is exposed in dorsal view above the right lateral surface of the skull, and some palatal elements are displaced posteriorly into the region of the pectoral girdle.

In addition to the excellent preservation of osteological elements, specific cranial areas of the fossil were identified during preparation as having a high potential for the preservation of soft tissues (see section 3.1). These regions are located in the posterior portion of the skull, near the supratemporal, jugal, and the lower jaw (Figs. 2B and 2C). The identification of these areas was initially based on their waxy appearance, distinctive coloration, as well as on macroscopic observations of aligned patterns visible on the fossil surface as elongated strips of potential soft tissue (Figs. 2D–G). These alignment patterns appear on the surface as a wrinkled texture.

4.2. Transmitted and polarized light microscopy

After about 20 days of EDTA treatment in fractions of CIP-0107-A, the glass slides mounted with the EDTA supernatant revealed

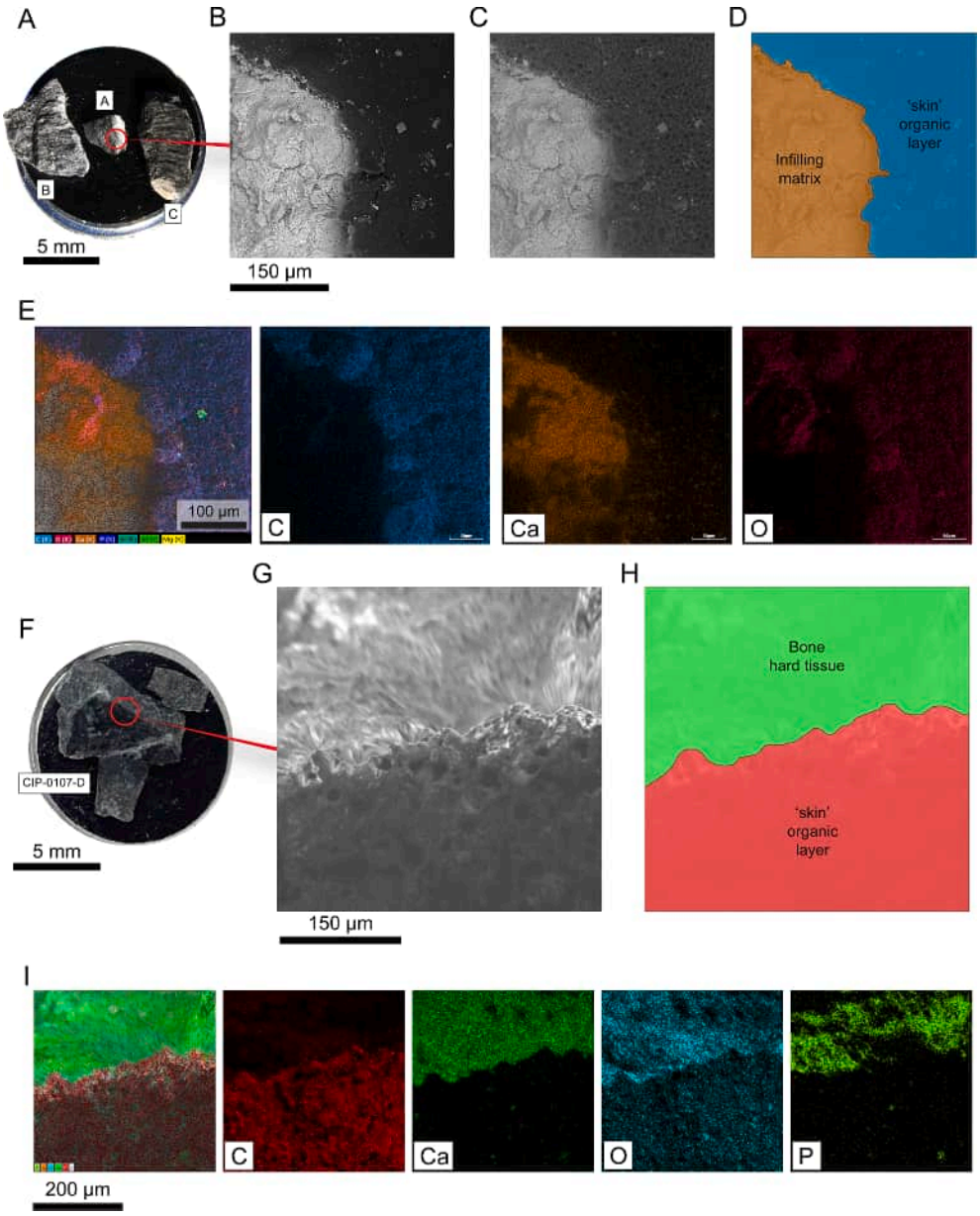

Fig. 6. SEM micrographs and EDS elemental composition analyses of untreated and uncoated fragments of CIP-0107. **A**, samples A, B, and C mounted on the SEM-stub. **B**, backscattered electron (BSE) image acquired at 799x magnification and 20 keV of CIP-0107-A. **C**, same micrograph as in (B) after EDS analysis, showing the extremely wrinkled (burned) organic surface of the skin-like layer in contact with the remaining infilling rock matrix region. **D**, interpretation of (B) showing the skin-like layer in contact with the infilling rock matrix. Colors correspond to elements in (E). **E**, elemental mapping of (B) showing carbon, calcium, and oxygen distributions. **F**, CIP-0107-D displaying high potential for soft-tissue preservation mounted on the SEM-stub. **G**, backscattered electron (BSE) image acquired at 799x magnification and 20 keV of F. **H**, interpretation of (G) showing the 'skin' organic layer in contact with bone tissue. Colors correspond to elements in (I). **I**, elemental mapping of (G) showing carbon, calcium, oxygen, and phosphorus distributions.

the presence of reticulated, net-like structures (Figs. 3D–L). These structures, identified under transmitted light microscopy, exhibit reticulated patterns that, in some cases, converge toward a central point (Fig. 3F). These net-like structures are brown-stained, and optically isotropic, showing no birefringence under cross-polarized light, consistent with the absence of double refraction which is typical of organic matter (Frandsen, 2016). Area measurements of the hollow regions of these structures range from 4.04 μm^2 to 64.44 μm^2, with a relatively high standard deviation (Figs. 3E, 3F and 3L), whereas the surrounding walls ('muri') measure an average width of 2.97 µm (range 1.19 µm–5.52 µm) with a low standard deviation (Fig. 3L). Additionally, fragments of the laminar, flexible, skin-like layer (~5 mm) were found in the beaker following EDTA treatment (Figs. 3B and Supplementary Material 1). Under the optical microscope, the skin-like layer shows dark, translucent zones, and some net-like brown-stained structures embedded in the layer (Figs. 9C-E).

Supplementary video related to this article can be found at https://doi.org/10.1016/j.cretres.2025.106305

Examination of the CIP-0107-A thin section revealed detailed features of the hard tissues of the exoccipital, soft-tissues, and matrix. This bone has not been previously examined histologically in ichthyosaurs, so no comparative data are available. Consequently, the interpretation presented here relies on the

microstructural organization observed in the CIP-0107-A thin section, and on general histological criteria applied from previous ichthyosaur studies (Anderson et al., 2019). Laminations were observed in the area identified and designated in this study as the mineralized integumentary component 'mic' (Figs. 4A-D), while the underlying bone exhibited a clear transition from an inner trabecular region to an outer compact layer of parallel-fibered bone (pfb). The CIP-0107-A thin section exhibits trabecular spaces infilled whit calcium carbonate ($CaCO_3$), which shows strong birefringence under cross-polarized light (Figs. 4B and 4E) (Frandsen, 2016). The microstructural organization of the pfb region, characterized by subparallel alignment of lamellae (Figs. 4D–E), confirms that this corresponds to bone tissue. Additionally, two small star-shaped structures were identified within the 'mic' (Fig. 3M). These structures exhibit a distinctive morphology, each with an approximate diameter of 5 μm, and no birefringence under cross-polarized light using a Lambda (λ) filter (Fig. 3N).

4.3. SEM-EDS

The SEM backscattered electron image of CIP-0107-C reveals superficial alignment patterns as a folded or undulating surface in the central region (Fig. 5B), which is an area that corresponds to the 'mic' described from CIP-0107-A thin section observations (Fig. 4C). Point elemental analysis in this area indicates a composition dominated by oxygen (48.17 %), carbon (39.90 %), and calcium (10.68 %), consistent with calcium carbonate composition (Fig. 5C). Trace amounts of silicon, magnesium, sulfur, phosphorus, and aluminum were also detected.

A portion of CIP-0107-A revealed two distinct regions (Fig. 6B): a thin, homogeneous dark layer interpreted as part of the skin-like layer, and a lighter region corresponding to the rock matrix (Fig. 6D). EDS analysis of the dark region showed significant wrinkling due to the burn effect associated with EDS application to uncoated organic materials, similar to degradation of non-conductive materials under high voltage in SEM (Thermo Fisher Scientific, n.d.) (Fig. 6C), and revealed enrichment in carbon and oxygen, with no detectable calcium present. In contrast, the rock matrix showed high calcium enrichment, consistent with a calcium carbonate composition (Fig. 6E).

CIP-0107-D exhibited an organic region and underlying mineralized bone tissue (Figs. 6F–H). EDS analysis of the bone tissue showed enrichment in calcium and phosphorus, consistent with calcium phosphate, while the adjacent organic layer exhibited carbon enrichment (Fig. 6I). This contrasts with the mineralized region in CIP-0107-A (Figs. 6C–E), where EDS revealed calcium carbonate composition in the surrounding matrix, indicating variation in mineral composition across distinct parts of the specimen.

A fragment of the laminar, flexible, skin-like layer (~5 mm) resulting from EDTA demineralization of a fraction of CIP-0107-A (Fig. 7A and Supplementary Material 1) is predominantly organic in nature, with carbon and oxygen accounting for 99.67 % of its elemental composition (Figs. 7C and 7E). This composition is consistent with fossilized organic matter, which typically shows elevated C and O proportions, and lacks detectable calcium, distinguishing it from carbonate-based mineral phases (Cadena, 2020). Also, as seen in the SEM analysis of CIP-0107-A (Fig. 6C), the skin-like layer (Fig. 7B) also transformed into a wrinkled surface texture resulting from EDS analysis burn effect (Fig. 7D) (Thermo Fisher Scientific, n.d.).

The SEM-EDS analysis of the 'mic' observed in the CIP-0107-A thin section (Figs. 7F-H), revealed delicate, elongate structures embedded within a mineralized matrix, predominantly composed of calcite, as indicated by their exfoliation and the presence of calcium (Fig. 5C). EDS analysis of the embedded structures showed enrichment in carbon and oxygen, with an absence of calcium, confirming their organic composition (Figs. 7G–H). The elongate and tubular organic structures have an average width of 12.30 μm (ranging from 9.11 to 15.86 μm), with a relatively low standard deviation.

4.4. ATR-FTIR

The FTIR spectrum for the untreated CIP-0107-A fragment (Figs. 8E and 8F) exhibited characteristic absorption bands consistent with a carbonate-rich composition, at 1446, 1381, 871, and 713 cm^{-1} (Fig. 8A). The control matrix displayed a nearly identical profile, confirming a composition dominated by calcium carbonate ($CaCO_3$). Both samples also showed a band near 1022 cm^{-1}, which is not typically associated with the standard spectral profile of pure calcium carbonate (NIST). Although this band is located in the spectral region that typically corresponds to polysaccharides (Helm et al., 1991), it could be also related to phosphates (Schmitt and Flemming, 1998).

In contrast, a fraction of the skin-like layer, obtained from demineralization of a fraction of CIP-0107-A (Figs. 8C and 8D), displayed additional absorption bands that are not present in the untreated sample or control matrix. These include peaks at 2970, 1724, 1589, and 1234 cm^{-1}, as well as a band at 1141 cm^{-1} (Fig. 8B). Comparative spectra reported from modern algae and biofilms (Lindgren et al., 2011; Ammari et al., 2017; Lee et al., 2017) exhibited peaks at 1625, 1405, 1045, and 1022 cm^{-1}, with a partial to almost no overlap with the EDTA-treated sample spectra. Bands at 2970, 1724, 1589, and 1234 cm^{-1} were absent in these biological controls, underscoring spectral differences between modern algae, biofilms, and the skin-like layer.

4.5. Raman microspectroscopy

The Raman spectra obtained from different regions of a fragment of the skin-like layer, obtained from demineralization of a fraction of CIP-0107-A, revealed multiple distinct peaks particularly between 1000 and 1800 cm^{-1} (Fig. 9A). The brown-stained structure (Fig. 9D) exhibited the most complex spectrum, with well-defined peaks at approximately 1345 cm^{-1} and 1595 cm^{-1}, along with additional bands near 1260 cm^{-1}, 1450 cm^{-1}, and a weaker signal around 1700 cm^{-1}. Although affected by elevated baseline fluorescence, these bands were consistently observed only in this structure and not in other areas of the skin-like layer. The translucent area (Fig. 9C) showed a comparatively simpler spectrum, with peaks at 1345 cm^{-1} and 1595 cm^{-1}, and a moderate signal near 1260 cm^{-1}, while other bands were less well defined or absent. In contrast, the black structure (Fig. 9E) displayed a markedly simplified spectrum, with prominent peaks restricted to 1345 cm^{-1} and 1595 cm^{-1}, and no additional bands distinguishable from background levels. These two peaks were consistently present across all spectra from the structures and zones of the CIP-0107-A skin-like layer, and correspond to regions commonly identified as the disordered (D) and graphitic (G) bands in Raman analyses of carbon-rich materials (Tuinstra and Koenig, 1970; Beyssac et al., 2002; Brolly et al., 2016).

Comparative reference spectra included *Allosaurus fragilis* Marsh, 1877 bone tissue (Wiemann et al., 2018), eumelanin in fossil epidermis of a hadrosaur (Fabbri et al., 2020), a melanin film extracted from the *Rana esculenta* Linnaeus, 1758 liver (Capozzi et al., 2005), and a simulated kerogen spectrum based on peak positions from Brolly et al. (2016). Among these, the spectrum from the *Allosaurus fragilis* bone tissue (Fig. 9B) showed partial

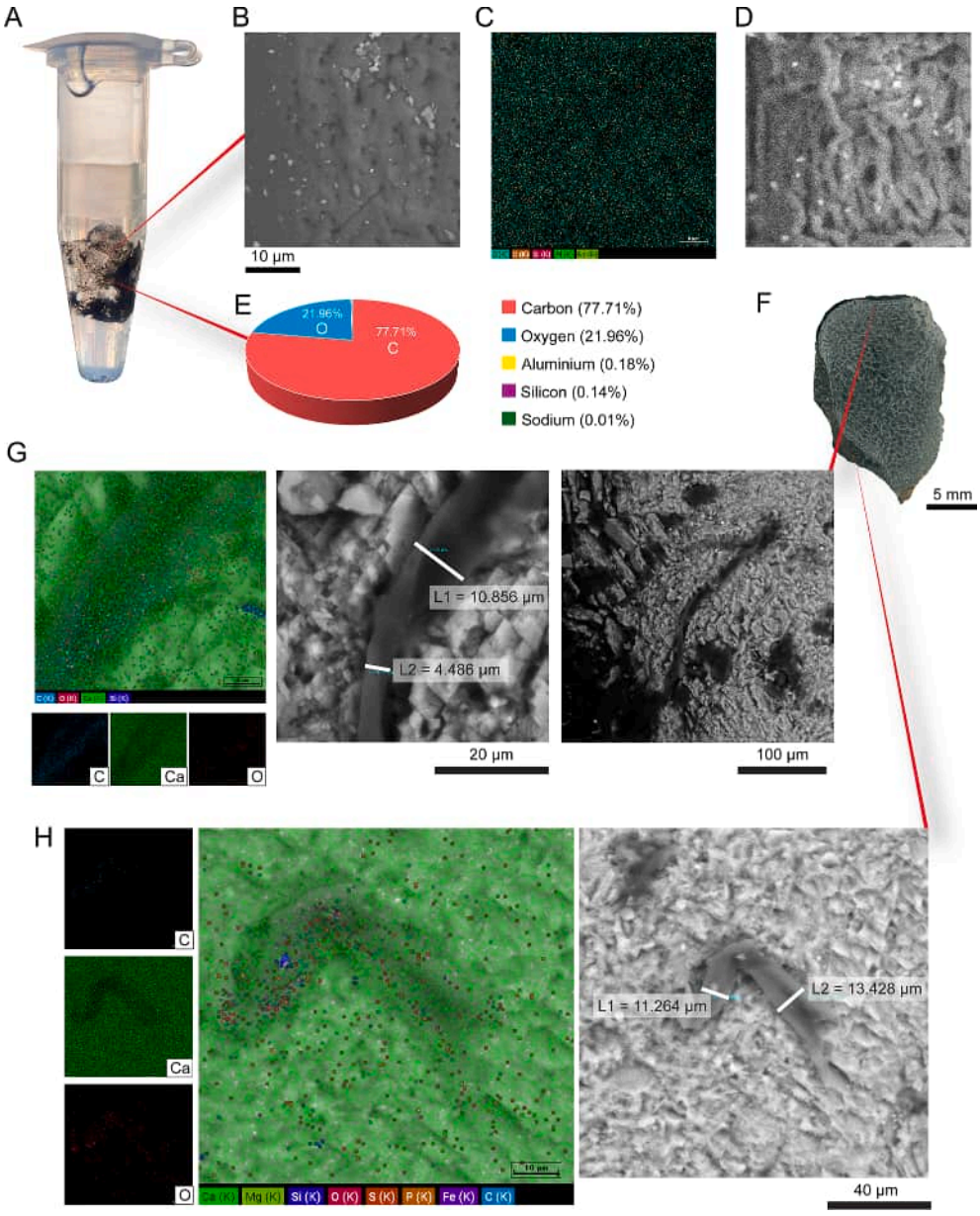

Fig. 7. SEM micrographs and EDS elemental composition analyses of CIP-0107-A skin-like layer and thin section. **A**, portion of CIP-0107-A after approximately 20 days of EDTA treatment, showing preservation of the skin-like layer. **B**, backscattered electron (BSE) image of (A) acquired at 7.05x magnification and 10 keV. **C**, elemental mapping of (B). **D**, same micrograph as in (B) after EDS analysis, showing the wrinkled (burned) organic surface of the skin-like layer. **E**, elemental composition of (A) indicating dominance of carbon and oxygen (Atomic %). **F**, thin section of CIP-0107-A. **G**, backscattered electron (BSE) image of (F) acquired at 10 keV and elemental mapping of an elongated, tubular, organic structure present in the upper mineralized integumentary component (mic) area of the thin section showing carbon, calcium, and oxygen distributions. **H**, backscattered electron (BSE) image acquired at 10 keV and elemental mapping of an elongated organic structure present in the lower mineralized integumentary component (mic) area of the thin section showing carbon, calcium, and oxygen.

resemblance to the brown-stained structure from CIP-0107-A, particularly in the presence of a prominent peak near ~1600 cm^{-1}, which was also the most intense feature in both spectra. Additional similarities include a band near ~1375 cm^{-1} (1345 cm^{-1} in skin-like layer), a feature near ~1260 cm^{-1}, and a subtle signal around ~1700 cm^{-1}. The eumelanin in epidermis spectrum exhibited peaks near 1275 cm^{-1}, ~1450 cm^{-1}, 1600 cm^{-1}, and 1690 cm^{-1} overlapping in position with some of the bands observed in the brown-stained structure, except for the pronounced peak at 1350 cm^{-1}. The melanin film spectrum showed a smoother profile with limited peak definition, but with a general shape closely resembling that of the simulated kerogen spectrum, characterized by dominant intensity around 1350 and 1600 cm^{-1}. Unlike these simpler profiles, the brown-stained region of CIP-0107-A displayed a more complex set of peaks particularly distributed across the 1200–1700 cm^{-1} range.

5. Discussion

5.1. Macroscopic morphology of the soft-tissue

Various studies have advanced our understanding of ichthyosaur soft tissues. Early interpretations proposed that fibrous textures represented fossilized collagen fibers (Lingham-Soliar, 1999), but given that this study relied exclusively on morphological observations, these structures were later reinterpreted as sedimentary structures and preparation marks (Smithwick et al., 2017). Nevertheless, post-mortem degradation of integumentary layers

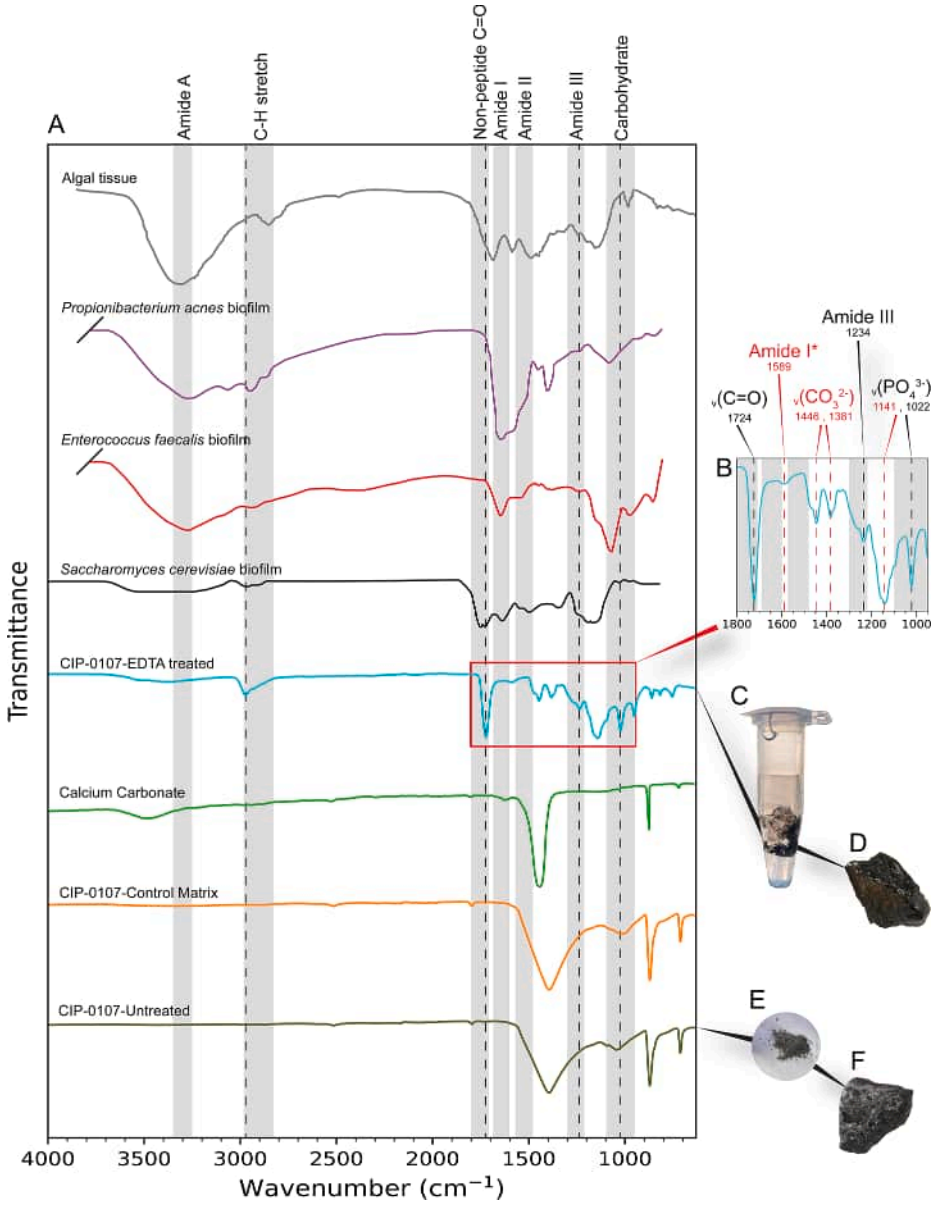

Fig. 8. FTIR spectra of CIP-0107 compared to mineral and biological controls. **A**, composite FTIR spectra (transmittance on the vertical axis, wavenumber on the horizontal axis) obtained from the analysis of different samples: Algal tissue (gray line) corresponding to *Hydrodictyon reticulatum* redrawn from Ammari et al. (2017); extant bacteria biofilms (purple, red and black lines) redrawn from Lee et al. (2017) and Lindgren et al. (2011); CIP-0107-A skin-like layer after treatment with EDTA (light blue line); calcium carbonate ($CaCO_3$) spectra (light green line) from NIST,; CIP-0107 control matrix (orange); and CIP-0107-A untreated (dark olive green). Gray bands show potential ranges of typical compounds based on Schmitt and Flemming (1998); Kong and Yu. (2007); Lee et al. (2017); Boatman et al. (2019); and Alfonso-Rojas and Cadena (2020). **B**, close-up of CIP-0107 untreated spectra, highlighting key peaks and functional group assignments. Interpreted bands include carbonate (νCO_3^{2-} at 1446 and 1381 cm^{-1}), phosphate (νPO_4^{3-} at 1141 and 1022 cm^{-1}), non-peptide C=O (1724 cm^{-1}), Amide III (1234 cm^{-1}), and a shifted (*) Amide I band (1589 cm^{-1}). **C**, skin-like layer coming from the CIP-0107-A-EDTA treated sample. **D**, portion of CIP-0107-A before EDTA treatment. **E**, powder of a portion of CIP-0107-A. **F**, portion of CIP-0107-A before being macerated in a sterilized agate mortar.

can generate undulating morphologies due to decay processes (Lingham-Soliar, 2015), and thus the wrinkles and ripples structures observed in some specimens could be interpreted as distortions of decaying integument caused by the loss of structural integrity, comparable to post-mortem deformation of skin in *Delphinus delphis* Linnaeus, 1758, and as interpreted in a specimen of *Stenopterygius* sp. (Lindgren et al., 2018). These morphologies closely resemble the alignment patterns observed in the soft-tissue areas preserved over the right lateral side of the CIP-0107 skull (Figs. 2D–G). Moreover, these alignment patterns are similar to soft tissue structures reported in European ichthyosaurs (e.g., Keller, 1992; Lindgren et al., 2018; Renesto et al., 2020), supporting the presence of soft-tissue preservation in this specimen.

5.2. Microscopic structural characterization of the soft-tissue

In well-preserved ichthyosaur specimens from better-known European deposits, distinct skin layers, such as epidermis, dermis, and the interface between them, have been observed (Lindgren et al., 2018, 2025; Bonnevier-Wallstedt et al., 2024). Additionally, star-shaped cells, likely melanophores, are frequently

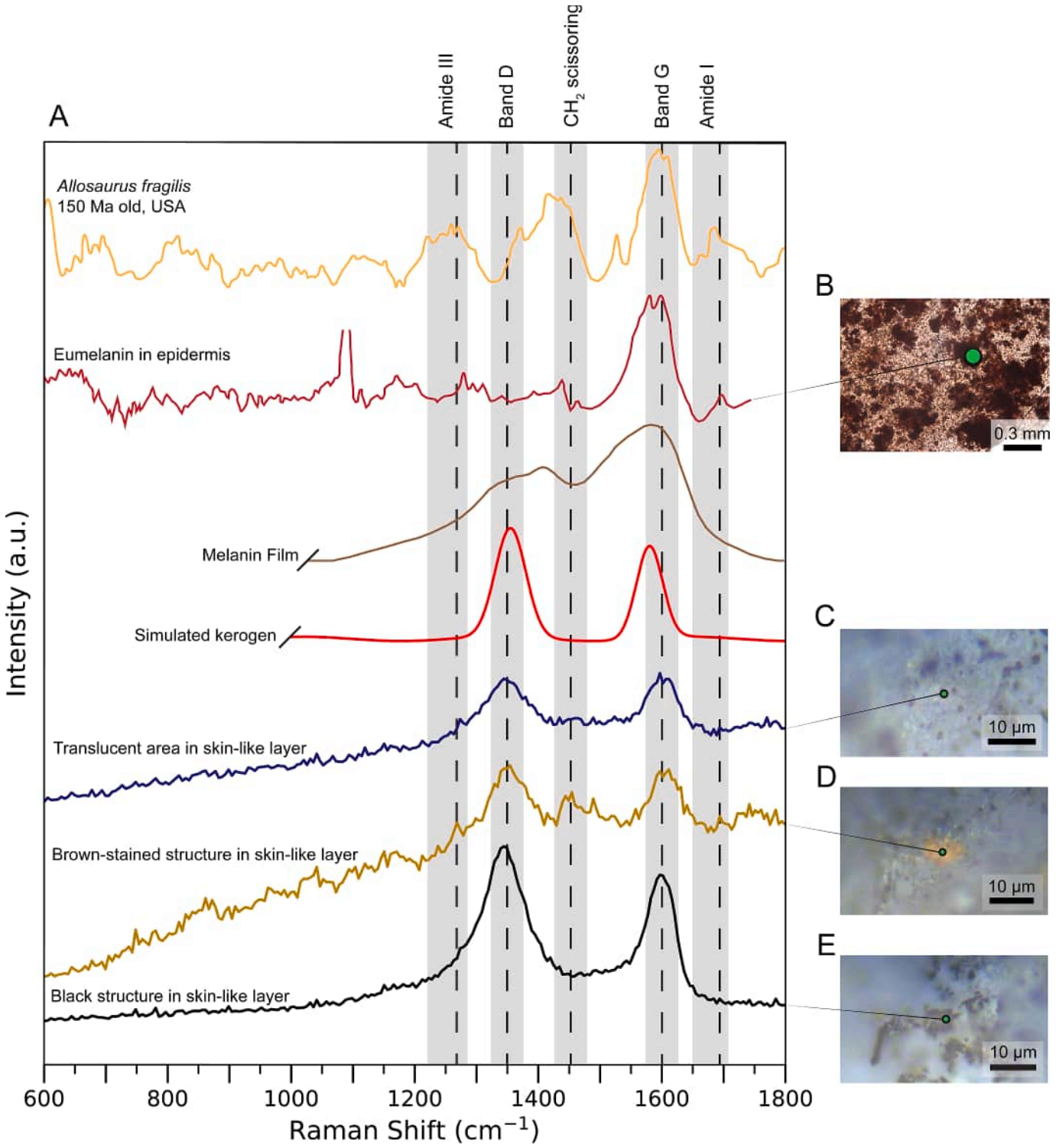

Fig. 9. Raman spectra of CIP-0107-A skin-like layer compared to organic and fossil reference materials. **A**, composite Raman spectra (intensity on the vertical axis, Raman shift on the horizontal axis) obtained from the analysis of different samples: *Allosaurus fragilis* bone tissue (150 Ma, USA) (yellow line, redrawn from Wiemann et al., 2018); eumelanin in fossil epidermis of an hadrosaur (dark red line, redrawn from Fabbri et al., 2020); melanin film extracted from the liver of *Rana esculenta* (dark brown, redrawn from Capozzi et al., 2005); simulated kerogen spectrum (red line, based on peak positions described in Brolly et al., 2016); and three spectra collected from CIP-0107-A skin-like layer: translucent region (blue line), brown-stained structure (golden brown line), and black structure (black line). Gray shaded bands indicate typical Raman shift ranges associated with Amide III, disordered (D) band, CH_2 scissoring, graphitic (G) band, and Amide I (based on Pawlak et al., 2008; Brolly et al., 2016; Wiemann et al., 2018). **B**, micrograph of formerly proteinaceous matrix with embedded melanocytes from a hadrosaur (taken from Fabbri et al., 2020). **C**, translucent region from the skin-like layer of CIP-0107-A. **D**, brown-stained structure from the skin-like layer of CIP-0107-A. **E**, black structure from the skin-like layer of CIP-0107-A. **Abbreviations**: **Ma**, Millions of years ago.

identified within the epidermis (Lindgren et al., 2018, 2025; Smithwick, 2019; De La Garza et al., 2023; Bonnevier-Wallstedt et al., 2024, and references therein). Laminations observed in the 'mic' of the CIP-0107-A thin section (Fig. 4D) are interpreted as original integumentary layering that was secondarily mineralized in calcium carbonate, and the trabecular spaces showing strong birefringence under cross-polarized light were infilled with calcium carbonate (Figs. 4B and 4E) despite the composition of bone tissue in calcium phosphate (Fig. 6I). This mineralization must have occurred early during diagenesis under localized geochemical conditions that favored rapid precipitation of calcite, potentially mediated by anaerobic microbial activity (see section 5.4. below). Moreover, within this 'mic' two approximately star-shaped structures, possibly melanophores (Figs. 3M–N), and thin elongated organic structures (Figs. 7G-H) are preserved offering additional evidence that the 'mic' may represent a structurally replaced integumentary zone.

The soft and flexible nature of the skin-like layer fragments remaining after EDTA demineralization of fractions of CIP-0107-A (Fig. 3B and Supplementary Material 1) bears a striking resemblance to the pliable remnants of the scaleless skin documented in an Early Jurassic ichthyosaur from Germany (Lindgren et al., 2018) and an Early Cretaceous fish from Colombia (Alfonso-Rojas and Cadena, 2020). Additionally, smooth, and homogeneous non-crystalline structures observed adjacent to the infilling rock matrix of CIP-0107-A (Figs. 6A-E), and in association with bone tissue of CIP-0107-D (Figs. 6F-I) are here interpreted as part of the skin-like layer. Although these samples were not treated with EDTA, the structures observed during the SEM wrinkled under EDS analysis (Figs. 6C and 7D), a response consistent with known energy effects on uncoated organic material (Thermo Fisher Scientific, n.d) during elemental mapping, and also observed in other specimens documented from the Paja Formation (Alfonso-Rojas and Cadena, 2020).

The net-like structures recovered from the supernatant following demineralization of CIP-0107-A fragments lack birefringence under cross-polarized light and exhibit a complex reticular morphology (Figs. 3D–L). Lack of birefringence is a feature typically related to crystalline structures found in anisotropic inorganic materials, and indicates a potential organic composition (Frandsen, 2016). A particular observation of the net-like structures is the brown-stained coloration. Although this coloration aligns with observations of amorphous organic matter (AOM), where coloration can range from translucent beige to brown depending on factors such as degree of agglomeration, preservation state, and material thickness (Pacton et al., 2011), the structures described here are not amorphous, since these exhibit a complex, highly organized morphology with well-defined 'muri' and hollows (Figs. 3E-G). Furthermore, this coloration contrasts with the expected black color of thermally altered organic matter from the Paja Formation, as this area is suggested to have a history of high thermal maturation (Gaona-Narvaez et al., 2013). Thus, the dark coloration likely reflects more than just optical artifacts. Brown-stained coloration of the net-like structures suggest the presence of N-heterocyclic polymers, such as melanoidins, formed through Maillard-type reactions as indicated by both experimental and fossil evidence (Hayase et al., 2008; Vistoli et al., 2013; Wiemann et al., 2018). The presence of this kind of pigment in the structures results in a yellowish-brown appearance, and it could be identified by Raman bands of advanced glycoxidation end-products (AGEs) (Pawlak et al., 2008; Wiemann and Briggs, 2022). Therefore, these organic net-like structures are regarded as fragments of keratinized stratified squamous epithelium, for instance from the stratum spinosum of the epidermis. The observed morphology, including the width of the 'muri' and dimensions of the hollow areas (Figs. 3E–G), is consistent with similar structures found in modern whales and dolphins, taxa with a gross anatomy comparable to ichthyosaurs (Reeb et al., 2007; Morales-Guerrero et al., 2017; Cozzi et al., 2017). Other net-like morphologies of comparable dimensions have been described in the fossil record, including specimens from the Posidonienschiefer Formation (Martill, 1987b), although early interpretations often attributed such patterns to microbial mats or biofilms. However, microbial biofilms typically produce amorphous networks with diffuse boundaries, and algae typically have hexagonal coenobium (Chou et al., 2006). In contrast, the net-like structures in CIP-0107 exhibit consistent wall thickness and boundary definition, with cylindrical rather than polygonal hollows.

Moreover, structures described in the epidermis of an ichthyosaur (Lindgren et al., 2018, fig. 2k) and a plesiosaur (Marx et al., 2025, fig. 2A) exhibit comparable net-like morphologies, which are homologous to the net-like structures observed in CIP-0107. These features represent remnants of the stratum spinosum or a structurally equivalent epidermal layer. This interpretation is consistent with experimental data showing that epidermal tissues from extant organisms can persist under simulated diagenetic conditions with minimal morphological deformation (Lindgren et al., 2018, fig. 9).

5.3. Elemental and chemical characterization of the soft-tissue

The skin-like layer fragments, obtained from the demineralization of fractions of CIP-0107-A, show distinct FTIR absorption bands not observed in the matrix or untreated fossil sample (Fig. 8), including peaks at 1234, 1589, and 1724 cm^{-1}, which correspond to Amide III, a potential shifted Amide I, and non-peptide carbonyl (C=O), respectively (Kong and Yu, 2007; Boatman et al., 2019; Alfonso-Rojas and Cadena, 2020). Additional peaks at 2970 cm^{-1} (attributed to CH_3/CH_2 asymmetric stretching; Lee et al., 2017; Boatman et al., 2019; Alfonso-Rojas and Cadena, 2020) and 1141–1022 cm^{-1} (located within a spectral region commonly associated with polysaccharide ring vibrations, but more consistent with phosphate based on peak position; Helm et al., 1991; Schmitt and Flemming, 1998) further distinguish this material from mineral or exogenous organic sources, such as bacterial biofilms or algal remains.

The possibility that this layer originates from a bacterial biofilm or algal mat is excluded based on the absence of strong hydroxyl group (-OH) absorption bands between 3700 and 3100 cm^{-1}, which are characteristic of polysaccharides commonly found in the cell walls of bacteria and algae (Ammari et al., 2017; Lee et al., 2017; Alfonso-Rojas and Cadena, 2020). Considering their organic composition (Figs. 6E, 6I, and 7E), the wrinkling pattern observed during EDS elemental analysis (Figs. 6C and 7D), and the unique FTIR absorption profile (Fig. 8B), this layer is strongly indicative of preserved epidermal tissue in CIP-0107.

Raman spectroscopy of the skin-like layer reveals a spectrum from a heterogeneous mixture of diagenetically altered organic residues (Figs. 9C–E), where the darkest particles (Fig. 9E) within the layer show intense bands at ~1345 cm^{-1} and ~1595 cm^{-1}, corresponding to the disordered (D) and graphitic (G) bands, a signature typical of thermally mature carbonaceous compounds or kerogen (Tuinstra and Koenig, 1970; Beyssac et al., 2002; Brolly et al., 2016). In contrast, the brown-stained structure (Fig. 9D) and the translucent region (Fig. 9C) in the skin-like layer display additional peaks at ~1260 cm^{-1}, ~1450 cm^{-1}, and ~1700 cm^{-1}. The peak at ~1260 cm^{-1} is consistent with Amide III, associated with C–N stretching and N–H bending (Pawlak et al., 2008; Wiemann et al., 2018). The peak at ~1450 cm^{-1} can be attributed to CH_2 scissoring or deformation vibrations, which are typical of amino

acid side chains and lipoxidation products (Pawlak et al., 2008). Finally, the peak at ~1700 cm^{-1} is assigned either to Amide I or to non-peptidic carbonyl (C=O) stretching arising from aldehydes or crosslinked AGE-related residues (Brolly et al., 2016; Wiemann et al., 2018).

Raman spectra with D and G bands could be interpreted in different ways, such as eumelanin pigments in extant tissues, carbon-based manufactured pigment, kerogen, or even fossilized melanosome-rich tissues (Rossi et al., 2024). The distribution of the heterogeneous mixture present in the skin-like layer of CIP-0107 suggests a gradient of molecular preservation, in which different zones or structures represent distinct stages of organic transformation. The translucent areas, exhibiting weak but detectable amide and CH-related bands, likely correspond to regions where original proteinaceous compounds have only undergone partial degradation, consistent with early-stage glycoxidation and lipoxidation products (Pawlak et al., 2008). The brown-stained structure (Fig. 9D) displays a richer molecular profile, including Amide III, CH_2 deformation, and non-peptidic carbonyl signals, consistent with the presence of crosslinked nitrogenous polymers such as advanced glycoxidation (AGEs) and advanced lipoxidation end-products (ALEs) (Pawlak et al., 2008; Wiemann et al., 2018). The black regions show exclusively the D and G bands characteristic of disordered and graphitic carbon, indicating that these zones have undergone more advanced diagenetic alteration, with full aromatization and kerogenization of the original organic matter. This spatial heterogeneity supports a model in which soft-tissue proteins are progressively transformed into increasingly recalcitrant carbonaceous compounds under varying microenvironmental conditions (Vistoli et al., 2013).

The Raman spectrum of the brown-stained structures (such as the net-like structures) closely resembles that of preserved bone organic component in *Allosaurus fragilis* (Wiemann et al., 2018), and of dermal structures in a non-avian dinosaur (Fabbri et al., 2020). These spectra are marked by a dominant intensity peak around ~1600 cm^{-1} and additional peaks absent in the spectra of pure kerogen, further supporting the presence of crosslinked residues derived from original proteins. Therefore, the net-like structures are interpreted as fragments of preserved epidermal tissue with a composition of N-heterocyclic polymers, such as melanoidins (causing the yellowish-brown coloration), which in fact increase their formation with time and temperature (Vistoli et al., 2013), consistent with diagenetic processes altering the original proteins, as mentioned above.

However, the model of the formation of AGEs/ALEs via oxidative polymerization catalyzed by iron and reactive oxygen species, leading to the transformation of amino acids into stable heterocycles (Wiemann et al., 2018) is inconsistent with the dysoxic to anoxic depositional environment of the Paja Formation, where no iron was detected in FTIR or EDS analyses. Instead, the mildly alkaline, microbially mediated conditions inferred from the concretionary carbonate context, combined with phosphate availability (see 5.4. section below), point toward a non-oxidative Maillard-type mechanism (Vistoli et al., 2013), capable of producing similar N-heterocyclic compounds in the absence of oxygen. This model could be supported by the presence of phosphate peaks in FTIR and the molecular complexity revealed by Raman spectra, particularly in the brown-stained structures.

The elongate organic structures observed in the CIP-0107-A thin section (Figs. 7G–H) present interpretative challenges. Although their morphology and size are comparable to blood vessels documented in modern dolphins (Cozzi et al., 2017, fig. 2.9), these structures lack key preservational features typically associated with fossilized vascular tissues. Notably, they do not exhibit iron enrichment, which is commonly detected in fossil blood vessels due to hemoglobin breakdown (Schweitzer et al., 2014; Cadena, 2016; Ullmann et al., 2019). This absence raises doubts as to their vascular origin. These structures are relatively thin (approximately less than a 1 μm), which may account for the attenuated carbon signal observed during SEM-EDS analysis. As EDS relies on the detection of characteristic X-rays emitted from a specimen upon electron bombardment, the strength of the detected signal is proportional to the volume and exposed surface area of the target material (Goldstein et al., 2018). Alternatively, their size and morphology are consistent with microbial or fungal channels, as previously suggested for similar structures in fossil contexts (Martill, 1987b). However, definitive identification requires further investigation.

5.4. Taphonomic and paleoenvironmental implications of soft-tissue preservation

The taphonomic processes observed in the Paja Formation exemplify those found in Konservat-Lagerstätten environments, where unique depositional and diagenetic conditions promote exceptional fossil preservation (Seilacher et al., 1985). The articulated nature of many Paja Formation fossil specimens, including nearly complete and articulated marine reptile skeletons, turtles with eggs, turtle hatchlings, and potential lower jaw buccal connective tissue in an ichthyosaur (Cadena et al., 2019; Alfonso-Rojas and Cadena, 2020; Cortés et al., 2021; Palma-Castro et al., 2023), strongly supports rapid burial in anoxic conditions with minimal disturbance and an absence of benthic bioturbation (Noè and Gómez-Pérez, 2020).

The paleoenvironment of the Paja Formation reflects a relatively deep (~60–130 m) epicontinental sea characterized by dysoxic to anoxic bottom waters, low-energy sedimentation, and highly water-saturated sediments (Noè and Gómez-Pérez, 2020). The burial of CIP-0107 likely occurred as it sank into these soft sediments, paralleling mechanisms hypothesized for the Posidonienschiefer Formation (Martill, 1993; Nichols, 2023). However, differing from that case, where soft-tissue preservation is linked to phosphatization near a fluctuating redox boundary (Sinha et al., 2021; De La Garza et al., 2023; Muscente et al., 2023; Marx et al., 2025), the persistent anoxic conditions of the Paja Formation, lack of benthic fauna, and sedimentological features suggest a distinct taphonomic model from the Posidonienschiefer Formation. While the soft substrate likely prevented disarticulation of the CIP-0107 elements embedded in the sediment, partial degradation of the exposed upper surface of the specimen may account for the loss of skeletal components prior to final burial (Fig. 10). This preservational scenario, driven by in situ sinking and rapid burial, contrasts with the widely cited “bloat and float” model, which is unlikely in settings deeper than 50 m (Etayo-Serna, 1968; Schäfer, 1972; Reisdorf et al., 2012), such as the estimated depths of the Paja Sea (Noè and Gómez-Pérez, 2020).

Beyond rapid burial, the preservation of CIP-0107 is best explained by involving oxygen starved microbial activity and the formation of early diagenetic carbonate concretions. The partial three-dimensional preservation of the skull, partial articulation of the bones, and presence of soft-tissue traces suggest that anaerobic microbial communities greatly influenced fossil preservation. In dysoxic-anoxic conditions, microbial biofilms, especially those formed by sulfate-reducing bacteria, create localized microenvironments that stabilize decaying tissues, trap ions, and elevate pH, thereby initiating early mineralization (Dhami et al., 2023; Bonnevier-Wallstedt et al., 2024). These biofilms facilitate the precipitation of authigenic carbonate ($CaCO_3$) within hours, days or weeks of burial, encapsulating the organism and shielding it from further decay, compaction, and destruction. This process

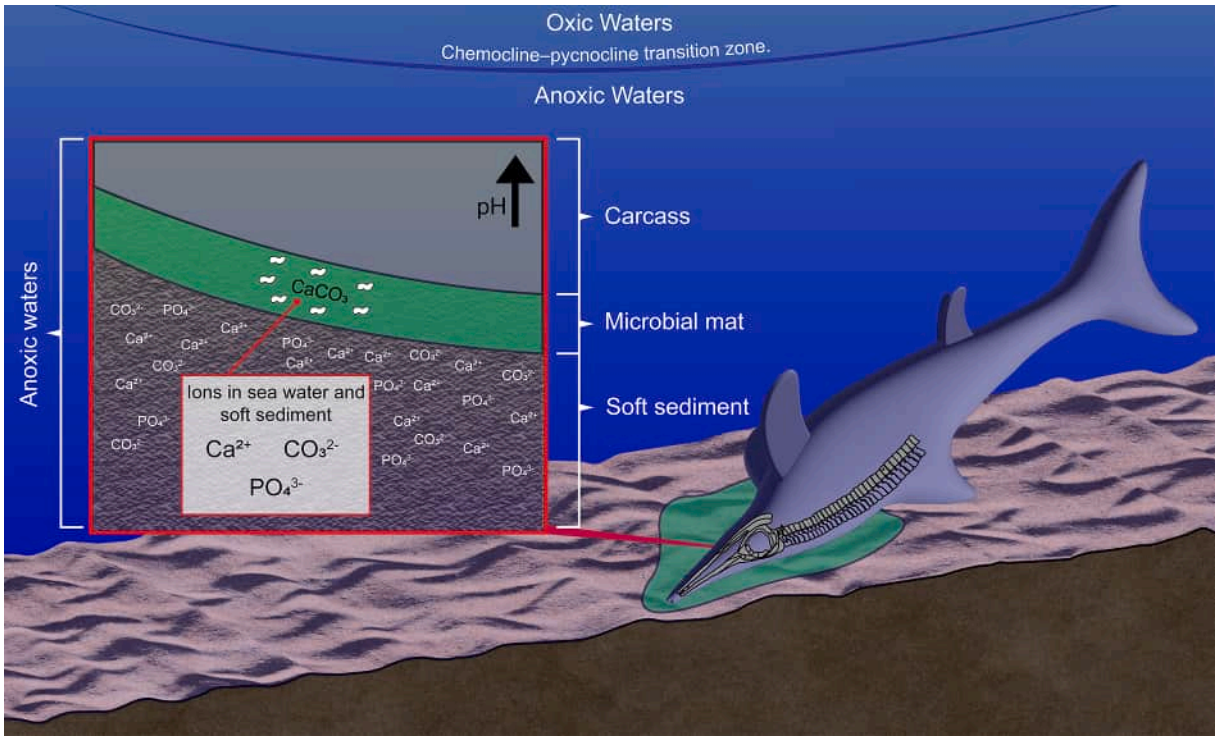

Fig. 10. Taphonomic model for the fossilization of CIP-0107. After death, the ichthyosaur carcass sank to the seafloor, where soft, water-saturated muds allowed partial burial and limited disturbance. An anoxic water column and the presence of a chemocline–pycnocline transition zone at depth prevented bioturbation and the settlement of encrusting organisms. Anaerobic microbial mats, potentially dominated by sulfate-reducing bacteria, developed between the carcass and the sediment creating a localized alkaline microenvironment that promoted early soft-tissue stabilization through the precipitation of calcium carbonate ($CaCO_3$). These microenvironmental conditions, particularly the elevated alkalinity and availability of phosphate, may have further favored molecular preservation via the formation of AGEs and ALEs. The result was the formation of a carbonate concretion that encapsulated the remains, shielding them from further decay and diagenetic alteration. Oxic-anoxic waters and chemocline–pycnocline transition zone indicated; water depths not to scale.

leads to the production of carbonate concretions that function as a geochemical capsule, preserving both morphological and molecular features.

The persistent bottom-water anoxia of the Paja Formation was likely caused by a combination of regional transgressive events and local paleoceanographic conditions. These included strong water column stratification separating oxygenated surface waters from dysoxic–anoxic bottom water layers, a tectonically restricted epicontinental basin that limited deep-water circulation, high global temperatures that enhanced nutrient recycling, and reduced oxygen solubility under greenhouse conditions (Meyer & Kump, 2008; Gaona-Narvaez et al., 2013; Noè & Gómez-Pérez, 2020). Together, these factors contributed to optimal conditions for fossil preservation in the Paja Formation sediments. This microbially mediated carbonate pathway differs from phosphatization models typical of other marine Konservat-Lagerstätten, highlighting the underexplored scientific potential of the Paja Formation to yield exceptionally preserved soft tissues in low-latitude marine settings that remain poorly represented in studies of soft-tissue fossilization. Moreover, its significance extends beyond latitude: the Paja Formation provides a window into the Lower Cretaceous Gap, a critical interval lacking well-preserved marine vertebrate Lagerstätten globally (Gómez-Pérez and Noè, 2017; Noè & Gómez-Pérez, 2020).

Future research should include SEM-EDS analyses at lower beam energies (2–5 keV) to enhance the detection of potential melanosomes in the skin-like layer (J. Lindgren, pers. comm.), transmission electron microscopy (TEM), and advanced molecular techniques like time-of-flight secondary ion mass spectrometry (ToF-SIMS) to provide more conclusive insights into the composition and origin of the preserved tissues.

6. Conclusions

This study is the first to characterize the morphology and composition of preserved soft-tissues in an ichthyosaur from the Lower Cretaceous (Barremian-Aptian) of Colombia. It also represents the first documented report of integumentary tissue preservation in a Cretaceous marine reptile from northern South America. Through the application of multiple analytical techniques including transmitted and polarized light microscopy, SEM-EDS, ATR-FTIR spectroscopy, and Raman microspectroscopy, our findings indicate that the ichthyosaur CIP-0107 exhibits exceptional soft-tissue preservation. Net-like structures identified in the specimen are interpreted as fragments of the stratified squamous epithelium, from the stratum spinosum layer of the epidermis of the ichthyosaur with a composition of N-heterocyclic polymers. The skin-like layer corresponds to preserved integumentary tissues, wherein original proteins have undergone diagenetic transformation into geochemically stable polymers, including N-heterocyclic polymers and kerogen-like substances.

The remarkable preservation of CIP-0107 is best explained by a taphonomic model involving rapid burial in soft, ion-rich sediments (particularly calcium, carbonate, and phosphate), persistent dysoxic to anoxic bottom-water conditions, and microbial biofilm activity that created localized alkaline geochemical microenvironments. These processes led to the formation of early diagenetic carbonate concretions that preserved the ichthyosaur in

exceptional fidelity. This model contrasts with soft-tissue preservation based on phosphatization under a sediment-water interface with a fluctuating redox boundary. This study thereby expands our understanding of soft-tissue preservation in marine vertebrates from low-latitude settings and underscores the scientific potential of the Paja Formation as a key source of paleobiological and taphonomic information from the Lower Cretaceous Gap. Finally, this study contributes to the field of molecular paleontology as it adds to the record of localities, specimens, and preservational environments that enhance our understanding of exceptional soft tissue preservation in the fossil record.

CRediT authorship contribution statement

Manuel F. Martinez-Motta: Writing – review & editing, Writing – original draft, Methodology, Investigation, Formal analysis. **Dirley Cortés:** Writing – review & editing, Writing – original draft, Funding acquisition, Conceptualization. **Erin E. Maxwell:** Writing – review & editing, Writing – original draft, Funding acquisition, Conceptualization. **Leslie F. Noè:** Writing – review & editing, Writing – original draft, Supervision, Funding acquisition. **Andrés Alfonso-Rojas:** Writing – review & editing, Writing – original draft, Investigation. **Fredy H. Parra-Ruge:** Writing – review & editing, Methodology. **Edwin-Alberto Cadena:** Writing – review & editing, Writing – original draft, Visualization, Validation, Supervision, Resources, Project administration, Methodology, Investigation, Funding acquisition, Formal analysis, Data curation, Conceptualization.

Author agreement statement

We the authors declare that this manuscript is original, has not been published before and is not currently being considered for publication elsewhere.

We confirm that the manuscript has been read and approved by all named authors and that there are no other persons who satisfied the criteria for authorship but are not listed. We further confirm that the order of authors listed in the manuscript has been approved by all of us.

We understand that the Corresponding Author is the sole contact for the Editorial process. He is responsible for communicating with the other authors about progress, submissions of revisions and final approval of proofs.

Declaration of competing interest

The authors declare the following financial interests/personal relationships which may be considered as potential competing interests:

M. Martínez and L.F. Noè obtained funding by the Facultad de Ciencias, Universidad de los Andes grant number INV-2020-105-2073.

E.E. Maxwell obtained partial funding from MWK seed funding for the preparation of the specimen.

A. Alfonso-Rojas is funded by the Gates Cambridge Trust.

D. Cortés is supported by BESS-NEO program, NSERC CREATE 46283-2015, the Smithsonian Tropical Research Institute, the Anders Foundation, the 1923 Fund, and Gregory D. and Jennifer Walston Johnson, the Fonds de recherche Nature et technologies Québec (FRQNT #302515), the Redpath Museum's Delise Alison Award-2019, the Sigma Xi Grant-in-aid-of-Research, Canada-2019 (GIAR), the Quebec Center for Biodiversity Science excellence award-2019, 2024 (QCBS), the Society of Systematic Biologists Graduate Student Research Award (2021) (GSRA), the Redpath Museum's Class of 66 Award 2022, and the McGill's Faculty of Science Graduate Mobility Awards (2021), 2023, McGill's Walter Hitschfeld Award 2024, and the CIP.

E-A. Cadena obtained funding for analyses and research of this Project from Dirección de Investigaciones e Innovación, Universidad del Rosario, Proyectos de Investigación (grant IV-FMD001, 2022).

Acknowledgements

We thank M.L. Parra-Ruge (CIP), J.D.D. Parra-Ruge (CIP), J. Pardo-Pérez (UMAG), and I.S. Lorentz (RedCode) for their dedication and efforts during the excavation of CIP-0107. Special thanks to staff at the CIP for their assistance with collection access and soft-tissue sampling. We also thank Y.C. Parra-Lamus for partial preparation of the specimen. Thanks for technical support provided by InClay, for SEM-EDS measurements, and MicroCore, a facility that is supported by the Vicepresidency for Research and Creation of the Universidad de los Andes. Thanks to A. Jiménez, Laboratory Technician, Department of Geosciences, Universidad de los Andes, for assistance in preparing the thin section, and J. Correa, Department of Chemistry, Universidad de los Andes, for support with the FTIR and Raman measurements. Special thanks to J. Lingren (Lund University) for opinions at an early stage of this project, B. Eickmann (Universidad de los Andes) for comments over the manuscript, C. Jaramillo (STRI), and H.C.E. Larsson (McGill) for discussion. We thank Dr. Lene Liebe Delsett and an anonymous reviewer for their constructive comments that helped substantially improve this manuscript. This work was undertaken as the undergraduate thesis project of M.F. Martinez-Motta, under the supervision of L.F. Noè and E.A. Cadena. Preparation of CIP-0107 was partially financed by MWK seed funding to E.E. Maxwell. This research was funded by the Facultad de Ciencias, Universidad de los Andes grant number INV-2020-105-2073 (to L.F. Noè); Dirección de Investigaciones e Innovación, Universidad del Rosario, Proyectos de Investigación (grant IV-FMD001, 2022 to E.A. Cadena). A. Alfonso-Rojas is funded by the Gates Cambridge Trust. D. Cortés was supported by BESS-NEO program, NSERC CREATE 46283-2015, the Smithsonian Tropical Research Institute, the Anders Foundation, the 1923 Fund, and Gregory D. and Jennifer Walston Johnson, the Fonds de recherche Nature et technologies Québec (FRQNT #302515), the Redpath Museum's Delise Alison Award-2019, the Sigma Xi Grant-in-aid-of-Research, Canada-2019 (GIAR), the Quebec Center for Biodiversity Science excellence award-2019, 2024 (QCBS), the Society of Systematic Biologists Graduate Student Research Award (2021) (GSRA), the Redpath Museum's Class of 66 Award 2022, and the McGill's Faculty of Science Graduate Mobility Awards (2021), 2023, McGill's Walter Hitschfeld Award 2024, and the CIP.

Data availability

Data will be made available on request.

References

Alfonso-Rojas, A., Cadena, E.A., 2020. Exceptionally preserved 'skin' in an Early Cretaceous fish from Colombia. PeerJ 8, e9479. https://doi.org/10.7717/peerj.9479.

Ammari, T.G., Al-Atiyat, M., Abu-Nameh, E.S., Ghrair, A., Jaradat, D.S., Abu-Romman, S., 2017. Bioremediation of cadmium-contaminated water systems using intact and alkaline-treated alga (*Hydrodictyon reticulatum*) naturally grown in an ecosystem. International Journal of Phytoremediation 19 (5), 453–462. https://doi.org/10.1080/15226514.2016.1244165.

Anderson, K.L., Druckenmiller, P.S., Erickson, G.M., Maxwell, E.E., 2019. Skeletal microstructure of *Stenopterygius quadriscissus* (Reptilia, Ichthyosauria) from the Posidonienschiefer (Posidonia Shale, Lower Jurassic) of Germany. Palaeontology 62 (3), 433–449. https://doi.org/10.1111/pala.12408.

Bardet, N., Fernández, M., 2000. A new ichthyosaur from the Upper Jurassic lithographic limestones of Bavaria. Journal of Paleontology 74 (3), 503–511. https://doi.org/10.1666/0022-3360(2000)074<0503:aniftu>2.0.co;2.

Benavides-Cabra, C.D., Páramo-Fonseca, M.E., Palma-Castro, H.D., Narváez-Rincón, J.A., Ramos-Clavijo, M.P., 2023. Stratigraphic distribution of marine vertebrates from the Arcillolitas Abigarradas Member (Paja Formation) of the Villa de Leiva–Sáchica-Sutamarchán region, Boyacá, Colombia. Earth Sciences Research Journal 27 (3), 211–226. https://doi.org/10.15446/esrj.v27n3.108292.

Benavides-Cabra, C.D., Garavito-Camacho, R.A., Páramo-Fonseca, M.E., Pomar, D.E., 2025a. A new brachaucheniine pliosaurid (Plesiosauria, Pliosauridae) from the upper Aptian of Villa de Leyva, Boyacá, Colombia. Historical Biology 1–27. https://doi.org/10.1080/08912963.2025.2580967.

Benavides-Cabra, C.D., Páramo-Fonseca, M.E., Narváez-Rincón, J.A., Pomar, D.E., 2025b. A large lamniform shark from the Aptian of Villa de Leiva (Boyacá, Colombia), based on the first Lower Cretaceous shark specimen preserving both teeth and vertebrae. Cretaceous Research, 106211. https://doi.org/10.1016/j.cretres.2025.106211.

Beyssac, O., Goffé, B., Chopin, C., Rouzaud, J.N., 2002. Raman spectra of carbonaceous material in metasediments: a new geothermometer. Journal of Metamorphic Geology 20 (9), 859–871. https://doi.org/10.1046/j.1525-1314.2002.00408.x.

Boatman, E.M., Goodwin, M.B., Holman, H.Y.N., Fakra, S., Zheng, W., Gronsky, R., Schweitzer, M.H., 2019. Mechanisms of soft tissue and protein preservation in *Tyrannosaurus rex*. Scientific Reports 9 (1), 15678. https://doi.org/10.1038/s41598-019-51680-1.

Bonnevier-Wallstedt, I., Sjövall, P., Thuy, B., De La Garza, R.G., Eriksson, M.E., Lindgren, J., 2024. Skin anatomy, bone histology and taphonomy of a Toarcian (Lower Jurassic) ichthyosaur (Reptilia: Ichthyopterygia) from Luxembourg, with Implications for Paleobiology. Diversity 16 (8), 492. https://doi.org/10.3390/d16080492.

Brolly, C., Parnell, J., Bowden, S., 2016. Raman spectroscopy: Caution when interpreting organic carbon from oxidising environments. Planetary and Space Science 121, 53–59. https://doi.org/10.1016/j.pss.2015.12.008.

Brown, C.M., Henderson, D.M., Vinther, J., Fletcher, I., Sistiaga, A., Herrera, J., Summons, R.E., 2017. An exceptionally preserved three-dimensional armored dinosaur reveals insights into coloration and Cretaceous predator-prey dynamics. Current Biology 27 (16), 2514–2521. https://doi.org/10.1016/j.cub.2017.06.071.

Cadena, E.A., 2015. The first South American sandownid turtle from the Lower Cretaceous of Colombia. PeerJ 3, e1431. https://doi.org/10.7717/peerj.1431.

Cadena, E.A., 2016. Microscopical and elemental FESEM and Phenom ProX-SEM-EDS analysis of osteocyte-and blood vessel-like microstructures obtained from fossil vertebrates of the Eocene Messel Pit, Germany. PeerJ 4, e1618. https://doi.org/10.7717/peerj.1618.

Cadena, E.A., 2020. In situ SEM/EDS compositional characterization of osteocytes and blood vessels in fossil and extant turtles on untreated bone surfaces; different preservational pathways microns away. PeerJ 8, e9833. https://doi.org/10.7717/peerj.9833.

Cadena, E.A., Parham, J.F., 2015. Oldest known marine turtle? A new protostegid from the Lower Cretaceous of Colombia. PaleoBios 32, 1–42. https://doi.org/10.5070/p9321028615.

Cadena, E.A., Parra-Ruge, M.L., Parra-Ruge, J.D., Padilla-Bernal, S., 2019. A gravid fossil turtle from the Early Cretaceous reveals a different egg development strategy to that of extant marine turtles. Palaeontology 62, 533–545. https://doi.org/10.1111/pala.12413.

Capozzi, V.I.T.O., Perna, G., Gallone, A., Biagi, P.F., Carmone, P., Fratello, A., Guida, D., Zanna, P., Cicero, R., 2005. Raman and optical spectroscopy of eumelanin films. Journal of Molecular Structure 744, 717–721. https://doi.org/10.1016/j.molstruc.2004.11.074.

Carballido, J.L., Pol, D., Parra-Ruge, M.L., Padilla Bernal, S., Páramo-Fonseca, M.E., Etayo-Serna, F., 2015. A new Early Cretaceous brachiosaurid (Dinosauria, Neosauropoda) from northwestern Gondwana (Villa de Leiva, Colombia). Journal of Vertebrate Paleontology 35 (5), e980505. https://doi.org/10.1080/02724634.2015.980505.

Carrillo-Briceño, J.D., Parra, J.D., Luque, J., 2019. A new lamniform shark *Protolamna ricaurtei* sp. nov. from the Lower Cretaceous of Colombia. Cretaceous Research 95, 336–340. https://doi.org/10.1016/j.cretres.2018.12.007.

Chou, J.Y., Chang, J.S., Wang, W.L., 2006. *Hydrodictyon reticulatum* (Hydrodictyaceae, Chlorophyta), a new recorded genus and species of freshwater macroalga in Taiwan. Bioformosa 41 (1), 1–8.

Cleland, T.P., Schroeter, E.R., Zamdborg, L., Zheng, W., Lee, J.E., Tran, J.C., Bern, M., Duncan, M.B., Lebleu, V.S., Ahlf, D.R., Thomas, P.M., Kalluri, R., Kelleher, N.L., Schweitzer, M.H., 2015. Mass spectrometry and antibody-based characterization of blood vessels from *Brachylophosaurus canadensis*. Journal of Proteome Research 14, 5252–5262. https://doi.org/10.1021/acs.jproteome.5b00675.

Cortés, D., Páramo-Fonseca, M.E., 2018. Restos apendiculares de un ictiosaurio oftalmosáurido del Barremiano inferior de Villa de Leiva, Colombia. Boletin de Geologia 40, 15–30. https://doi.org/10.18273/revbol.v40n1-2018001.

Cortés, D., Larsson, H.C., Maxwell, E.E., Parra-Ruge, M.L., Patarroyo, P., Wilson, J.A., 2019. An early Cretaceous teleosauroid (Crocodylomorpha: Thalattosuchia) from Colombia. Ameghiniana 56 (5), 365–379. https://doi.org/10.5710/amgh.26.09.2019.3269.

Cortés, D., Maxwell, E.E., Larsson, H.C., 2021. Re-appearance of hypercarnivore ichthyosaurs in the Cretaceous with differentiated dentition: revision of '*Platypterygius*' *sachicarum* (Reptilia: Ichthyosauria, Ophthalmosauridae) from Colombia. Journal of Systematic Palaeontology 19 (14), 969–1002. https://doi.org/10.1080/14772019.2021.1989507.

Cortés, D., Parra-Ruge, M.L., Parra-Ruge, J.D., Deers-Potvin, A., Smith, A., Hoai-Nam, B., Larsson, H.C., 2023. Theropod dinosaur footprints from the Early Cretaceous of Colombia: walking dynamics and paleoenvironmental implications. Revista Facies 9, 1–17.

Cozzi, B., Mazzariol, S., Centelleghe, S., Mazzatenta, S., Della Salda, L., 2017. The skin of dolphins and its histological layers. In: Cozzi, B., Huggenberger, S., Oelschläger, H.A. (Eds.), Anatomy of dolphins: Insights into body structure and function. Academic Press, pp. 25–43.

Cremona, J., 2014. Extreme close-up photography and focus stacking. The Crowood Press, p. 176.

De La Garza, R.G., Sjövall, P., Hauff, R., Lindgren, J., 2023. Preservational modes of some ichthyosaur soft tissues (Reptilia, Ichthyopterygia) from the Jurassic Posidonia Shale of Germany. Palaeontology 66 (4), e12668. https://doi.org/10.1111/pala.12668.

Delair, J.B., 1966. Unusual preservation of fibrous elements in an ichthyosaur skull. Nature 212 (5062), 575–576. https://doi.org/10.1038/212575a0.

Delsett, L.L., Friis, H., Köbl-Ebert, M., Hurum, J.H., 2022. The soft tissue and skeletal anatomy of two Late Jurassic ichthyosaur specimens from the Solnhofen archipelago. PeerJ 10, e13173. https://doi.org/10.7717/peerj.13173.

Dhami, N.K., Greenwood, P.F., Poropat, S.F., Tripp, M., Elson, A., Vijay, H., Brosnan, L., Holman, A.I., Campbell, M., Hopper, P., Smith, L., Jian, A., Grice, K., 2023. Microbially mediated fossil concretions and their characterization by the latest methodologies: A review. Frontiers in Microbiology 14, 1225411. https://doi.org/10.3389/fmicb.2023.1225411.

Eriksson, M.E., De La Garza, R., Horn, E., Lindgren, J., 2022. A review of ichthyosaur (Reptilia, Ichthyopterygia) soft tissues with implications for life reconstructions. Earth-Science Reviews 226, 103965. https://doi.org/10.1016/j.earscirev.2022.103965.

Etayo-Serna, F., 1965. Sinopsis estratigráfica de la región de Villa de Leiva y zonas próximas. Boletin de Geologia 21, 19–32.

Etayo-Serna, F., 1968. El Sistema Cretáceo en la región de Villa de Leiva y zonas próximas. Geología Colombiana 5, 5–74.

Etayo-Serna, F., 1979. Zonation of the Cretaceous of central Colombia by ammonites, 2. Publicaciones Geológicas Especiales del Ingeominas, Bogotá, pp. 1–186.

Fabbri, M., Wiemann, J., Manucci, F., Briggs, D.E., 2020. Three-dimensional soft tissue preservation revealed in the skin of a non-avian dinosaur. Palaeontology 63 (2), 185–193. https://doi.org/10.1111/pala.12470.

Frandsen, A.F., 2016. *Polarized light microscopy* (NASA Technical Report No. KSC-E-DAA-TN37401). NASA, Kennedy Space Center, p. 29.

Gaona-Narvaez, T., Maurrasse, F.J.M., Etayo-Serna, F., 2013. Geochemistry, palaeoenvironments and timing of Aptian organic-rich beds of the Paja Formation (Curití, Eastern Cordillera, Colombia). Geological Society, London, Special Publications 382 (1), 31–48. https://doi.org/10.1144/sp382.6.

Goldstein, J.I., Newbury, D.E., Michael, J.R., Ritchie, N.W., Scott, J.H.J., Joy, D.C., 2018. Scanning electron microscopy and X-ray microanalysis. Springer, p. 550.

Gómez-Pérez, M., Noè, L.F., 2017. Cranial anatomy of a new pliosaurid *Acostasaurus pavachoquensis* from the Lower Cretaceous of Colombia, South America. Palaeontographica Abteilung A 310, 5–42. https://doi.org/10.1127/pala/2017/0068.

Hampe, O., 1992. Ein großwüchsiger Pliosauride (Reptilia: Plesiosauria) aus-der Unterkreide (oberes Aptium) von Kolumbien. Courier Forschungsinstitut Senckenberg 145, 1–25.

Hayase, F., Usui, T., Ono, Y., Shirahashi, Y., Machida, T., Ito, T., Nishitani, N., Shimohira, K., Watanabe, H., 2008. Formation mechanisms of melanoidins and fluorescent pyridinium compounds as advanced glycation end products. Annals of the New York Academy of Sciences 1126 (1), 53–58. https://doi.org/10.1196/annals.1433.009.

Helm, D., Labischinski, H., Schallehn, G., Naumann, D., 1991. Classification and identification of bacteria by Fourier-transform infrared spectroscopy. Microbiology 137 (1), 69–79. https://doi.org/10.1099/00221287-137-1-69.

IUGS [International Union of Geological Sciences], 2022. The first 100 IUGS geological heritage sites, p. 278 published by IUGS.

Jacobs, M.L., Martill, D.M., 2020. A new ophthalmosaurid ichthyosaur from the Upper Jurassic (Early Tithonian) Kimmeridge Clay of Dorset, UK, with implications for Late Jurassic ichthyosaur diversity. PLoS One 15 (12), e0241700. https://doi.org/10.1371/journal.pone.0241700.

Keller, T., 1992. "Weichteil-Erhaltung" bei großen Vertebraten (Ichthyosauriern) des Posidonienschiefers Holzmadens (Oberer Lias, Mesozoikum Süddeutschlands). Kaupia: Darmstädter Beiträge zur Naturgeschichte 1, 23–62.

Kimmig, J., Schiffbauer, J.D., 2024. A modern definition of Fossil-Lagerstätten. Trends in Ecology & Evolution 39 (7), 621–624. https://doi.org/10.1016/j.tree.2024.04.004.

Kong, J., Yu, S., 2007. Fourier transform infrared spectroscopic analysis of protein secondary structures. Acta Biochimica et Biophysica Sinica 39 (8), 549–559. https://doi.org/10.1111/j.1745-7270.2007.00320.x.

Lee, Y.C., Chiang, C.C., Huang, P.Y., Chung, C.Y., Huang, T.D., Wang, C.C., Chen, C., Chang, R.S., Liao, C.H., Reisz, R.R., 2017. Evidence of preserved collagen in an Early Jurassic sauropodomorph dinosaur revealed by synchrotron FTIR microspectroscopy. Nature Communications 8 (1), 14220. https://doi.org/10.1038/ncomms14220.

Lindgren, J., Uvdal, P., Engdahl, A., Lee, A.H., Alwmark, C., Bergquist, K.E., Nilsson, E., Ekström, P., Rasmussen, M., Douglas, D.A., Polcyn, M.J., Jacobs, L.L., 2011. Microspectroscopic evidence of Cretaceous bone proteins. PLoS One 6 (4), e19445. https://doi.org/10.1371/journal.pone.0019445.

Lindgren, J., Sjövall, P., Thiel, V., Zheng, W., Ito, S., Wakamatsu, K., Hauff, R., Kear, B.P., Engdahl, A., Alwmark, C., Eriksson, M.E., Jarenmark, M., Sachs, S., Ahlberg, P.E., Marone, F., Kuriyama, T., Gustafsson, O., Malmberg, P., Thomen, A., Rodríguez-Meizoso, I., Uvdal, P., Ojika, M., Schweitzer, M.H., 2018. Soft-tissue evidence for homeothermy and crypsis in a Jurassic ichthyosaur. Nature 564, 359–365. https://doi.org/10.1038/s41586-018-0775-x.

Lindgren, J., Lomax, D.R., Szász, R.-Z., Marx, M., Revstedt, J., Göltz, G., Sachs, S., De, R.G., Heingård, M., Jarenmark, M., Ydström, K., Sjövall, P., Osbæck, F., Hall, S.A., de, O., Eriksson, M.E., Alwmark, C., Marone, F., Liptak, A., Atwood, R., 2025. Adaptations for stealth in the wing-like flippers of a large ichthyosaur. Nature 1–18. https://doi.org/10.1038/s41586-025-09271-w.

Lingham-Soliar, T., 1999. Rare soft tissue preservation showing fibrous structures in an ichthyosaur from the Lower Lias (Jurassic) of England. Proceedings of the Royal Society of London. Series B: Biological Sciences 266 (1436), 2367–2373. https://doi.org/10.1098/rspb.1999.0933.

Lingham-Soliar, T., 2001. The ichthyosaur integument: skin fibers, a means for a strong, flexible and smooth skin. Lethaia 34 (4), 287–302. https://doi.org/10.1080/002411601753293042.

Lingham-Soliar, T., 2015. Integumental Taphonomy. In: The Vertebrate Integument, 2. Structure, Design and Function, pp. 263–293.

Lingham-Soliar, T., Plodowski, G., 2010. The integument of *Psittacosaurus* from Liaoning Province, China: taphonomy, epidermal patterns and color of a ceratopsian dinosaur. Naturwissenschaften 97, 479–486. https://doi.org/10.1007/s00114-010-0661-3.

Linnaeus, C., 1758. In: Systema naturæ per regna tria naturæ, secundum classes, ordines, genera, species, cum characteribus, differentiis, synonymis, locis, 10th ed 1. Laurentii Salvii.

Luque, J., Cortes, D., Rodriguez-Abaunza, A., Cardenas, D., de Dios Parra, J., 2020. Orithopsid crabs from the Lower Cretaceous Paja Formation in Boyacá (Colombia), and the earliest record of parasitic isopod traces in Raninoida. Cretaceous Research 116, 104602. https://doi.org/10.1016/j.cretres.2020.104602.

Marsh, O.C., 1877. Notice of new dinosaurian reptiles from the Jurassic Formation. American Journal of Science 3 (84), 514–516. https://doi.org/10.2475/ajs.s3-14.84.514.

Martill, D.M., 1987a. A taphonomic and diagenetic case study of a partially articulated ichthyosaur. Palaeontology 30 (3), 543–555.

Martill, D.M., 1987b. Prokaryote mats replacing soft tissues in Mesozoic marine reptiles. Modern Geology 11, 265–269.

Martill, D.M., 1988. Preservation of fish in the Cretaceous Santana Formation Brazil. Palaeontology 31 (1), 1–18.

Martill, D.M., 1993. Soupy substrates: a medium for the exceptional preservation of ichthyosaurs of the Posidonia Shale (Lower Jurassic) of Germany. Kaupia 2, 77–97.

Martill, D.M., 1995. An ichthyosaur with preserved soft tissue from the Sinemurian of southern England. Palaeontology 38 (4), 897–904.

Martin, T., Marugán-Lobón, J., Vullo, R., Martín-Abad, H., Luo, Z.X., Buscalioni, A.D., 2015. A Cretaceous eutriconodont and integument evolution in early mammals. Nature 526 (7573), 380–384. https://doi.org/10.1038/nature14905.

Martin, J.E., Suan, G., Suchéras-Marx, B., Rulleau, L., Schlögl, J., Janneau, K., Williams, M., Léna, A., Grosjean, A.-S., Sarroca, E., Perrier, V., Fernandez, V., Charruault, A.-L., Maxwell, E.E., Vincent, P., 2021. Stenopterygiids from the lower Toarcian of Beaujolais and a chemostratigraphic context for ichthyosaur preservation during the Toarcian Oceanic Anoxic Event, 514. Geological Society, London, Special Publications, pp. 153–172. https://doi.org/10.1144/sp514-2020-232.

Marx, M., Sjövall, P., Kear, B.P., Jarenmark, M., Eriksson, M.E., Sachs, S., Nilkens, K., Op De Beeck, M., Lindgren, J., 2025. Skin, scales, and cells in a Jurassic plesiosaur. Current Biology 35 (5), 1113–1120. https://doi.org/10.1016/j.cub.2025.01.001.

Maxwell, E.E., Dick, D., Padilla, S., Parra, M.L., 2016. A new ophthalmosaurid ichthyosaur from the Early Cretaceous of Colombia. Papers in Palaeontology 2 (1), 59–70. https://doi.org/10.1371/journal.pone.0241700.

Maxwell, E.E., Cortés, D., Patarroyo, P., Parra-Ruge, M.L., 2019. A new specimen of *Platypterygius sachicarum* (Reptilia, Ichthyosauria) from the Early Cretaceous of Colombia and its phylogenetic implications. Journal of Vertebrate Paleontology 39 (1), e1577875. https://doi.org/10.1080/02724634.2019.1577875.

Meyer, K.M., Kump, L.R., 2008. Oceanic euxinia in Earth history: causes and consequences. Annual Review of Earth and Planetary Sciences 36 (1), 251–288. https://doi.org/10.1146/annurev.earth.36.031207.124256.

Montoya-Arenas, D.M., Etayo-Serna, F., 2019. Formación La Paja: Descripción de la sección tipo. Influencia de los tapices microbiales en su génesis. In: Etayo-Serna, F. (Ed.), Estudios geológicos y paleontológicos sobre el Cretácico en la región del embalse del rio Sogamoso, Valle Medio del Magdalena. Compilación de los Estudios Geológicos Oficiales en Colombia XXIII. Servicio Geológico Colombiano, Bogotá, pp. 51–67.

Morales-Guerrero, B., Barragán-Vargas, C., Silva-Rosales, G.R., Ortega-Ortiz, C.D., Gendron, D., Martinez-Levasseur, L.M., Acevedo-Whitehouse, K., 2017. Melanin granules melanophages and a fully-melanized epidermis are common traits of odontocete and mysticete cetaceans. Veterinary Dermatology 28 (2), 1–8. https://doi.org/10.1111/vde.12392.

Motani, R., You, H., McGowan, C., 1996. Eel-like swimming in the earliest ichthyosaurs. Nature 382 (6589), 347–348. https://doi.org/10.1038/382347a0.

Muscente, A.D., Vinnes, O., Sinha, S., Schiffbauer, J.D., Maxwell, E.E., Schweigert, G., Martindale, R.C., 2023. What role does anoxia play in exceptional fossil preservation? Lessons from the taphonomy of the Posidonia Shale (Germany). Earth-Science Reviews 238, 104323. https://doi.org/10.1016/j.earscirev.2023.104323.

Nichols, G., 2023. Sedimentology and Stratigraphy, third ed. Wiley & Sons Ltd, p. 544.

NIST [National Institute of Standards and Technology, U.S. Department of Commerce]. (accessed November 26, 2024). Calcium carbonate (precipitated). NIST Chemistry WebBook, SRD, 69. webbook.nist.gov/cgi/cbook.cgi?ID=C471341&Units=SI&Mask=80#IR-Spec.

Noè, L.F., Gómez-Pérez, M., 2020. Plesiosaurs, palaeoenvironments, and the Paja Formation Lagerstätte of central Colombia: An overview, chapter 13. In: Gómez, J., Pinilla-Pachon, A.O. (Eds.), The Geology of Colombia, Volume 2 Mesozoic. Publicaciones Geológicas Especiales 36. Servicio Geológico Colombiano, pp. 441–483.

Noè, L.F., Gómez-Pérez, M., 2022. Giant pliosaurids (Sauropterygia; Plesiosauria) from the Lower Cretaceous peri-Gondwanan seas of Colombia and Australia. Cretaceous Research 132, e105122. https://doi.org/10.1016/j.cretres.2021.105122.

Pacton, M., Gorin, G.E., Vasconcelos, C., 2011. Amorphous organic matter—Experimental data on formation and the role of microbes. Review of Palaeobotany and Palynology 166 (3–4), 253–267. https://doi.org/10.1016/j.revpalbo.2011.05.011.

Paik, I.S., Kim, H.J., Huh, M., 2010. Impressions of dinosaur skin from the Cretaceous Haman Formation in Korea. Journal of Asian Earth Sciences 39 (4), 270–274. https://doi.org/10.1016/j.jseaes.2010.02.015.

Palma-Castro, H.D., 2024. Paleodiversidad de la flora fósil de la Formación La Paja, Cretácico Inferior de Colombia. Universidad Nacional de Colombia, p. 166. Unpublished Master's Thesis.

Palma-Castro, H.D., Cómbita-Romero, D.A., Cadena, E.A., Carvalho, M.R., Herrera, F., 2023. An Early Cretaceous *Sphenophyllum* or a hatchling turtle? Palaeontologia Electronica 26 (3), 1–10. https://doi.org/10.26879/1306.

Páramo-Fonseca, M.E., 1997. *Platypterygius sachicarum* (Reptilia, Ichthyosauria) nueva especie del Cretácico de Colombia. Revista Ingeominas 6, 1–12.

Páramo-Fonseca, M.E., Gómez-Pérez, M., Noé, L.F., Etayo-Serna, F., 2016. *Stenorhynchosaurus munozi*, gen. et sp. nov. a new pliosaurid from the Upper Barremian (Lower Cretaceous) of Villa de Leiva, Colombia, South America. Revista de la Academia Colombiana de Ciencias Exactas Físicas y Naturales 40 (154), 84–103. https://doi.org/10.18257/raccefyn.239.

Páramo-Fonseca, M.E., Benavides-Cabra, C.D., Gutiérrez, I.E., 2018. A new large Pliosaurid from the Barremian (Lower Cretaceous) of Sáchica, Boyacá, Colombia. Earth Sciences Research Journal 22 (4), 223–238. https://doi.org/10.15446/esrj.v22n4.69916.

Páramo-Fonseca, M.E., Benavides-Cabra, C.D., Gutiérrez, I.E., 2019a. A new specimen of *Stenorhynchosaurus munozi* Páramo-Fonseca et al., 2016 (Plesiosauria, Pliosauridae), from the Barremian of Colombia: new morphological features and ontogenetic implications. Journal of Vertebrate Paleontology 39, e1663426. https://doi.org/10.1080/02724634.2019.1663426.

Páramo-Fonseca, M.E., O'Gorman, J.P., Gasparini, Z., Padilla, S., Parra-Ruge, M.L., 2019b. A new late Aptian elasmosaurid from the Paja Formation, Villa de Leiva, Colombia. Cretaceous Research 99, 30–40. https://doi.org/10.1016/j.cretres.2019.02.010.

Páramo-Fonseca, M.E., García-Guerrero, J., Benavides-Cabra, C.D., Padilla-Bernal, S., Castañeda-Gómez, A.J., 2021. A benchmark specimen of *Muiscasaurus catheti* from the upper Aptian of Villa de Leiva, Colombia: new anatomical features and phylogenetic implications. Cretaceous Research 119, 104685. https://doi.org/10.1016/j.cretres.2020.104685.

Páramo-Fonseca, M.E., Benavides-Cabra, C.D., Palma-Castro, H.D., Castañeda-Gómez, A.J., 2023. Procumbent anterior premaxillary teeth in *Stenorhynchosaurus munozi* (Plesiosauria, Pliosauridae), evidence from new material. Earth Sciences Research Journal 27, 1–9. https://doi.org/10.15446/esrj.v27n1.105689.

Páramo-Fonseca, M.E., Benavides-Cabra, C.D., Garavito-Camacho, R.A., 2024. A new species of *Platypterygius* (Ophthalmosauridae) from the lower Barremian of Colombia and assessment of the species composition of the genus. Earth Sciences Research Journal 28 (2), 103–126. https://doi.org/10.15446/esrj.v28n2.112332.

Patarroyo, P., 2020. Barremian deposits of Colombia: a special emphasis on marine successions. In: Gómez, J., Pinilla-Pachon, A.O. (Eds.), The Geology of Colombia, 2. Mesozoic. Publicaciones Geológicas Especiales 36, Servicio Geológico Colombiano, pp. 403–439. Chapter 12.

Pawlak, A.M., Beattie, J.R., Glenn, J.V., Stitt, A.W., McGarvey, J.J., 2008. Raman spectroscopy of advanced glycation end products (AGEs), possible markers for progressive retinal dysfunction. Journal of Raman Spectroscopy 39 (11), 1635–1642. https://doi.org/10.1002/jrs.2011.

Reeb, D., Best, P.B., Kidson, S.H., 2007. Structure of the integument of southern right whales, *Eubalaena australis*. The Anatomical Record 290 (6), 596–613. https://doi.org/10.1002/ar.20535.

Reisdorf, A.G., Bux, R., Wyler, D., Benecke, M., Klug, C., Maisch, M.W., Fornaro, P., Wetzel, A., 2012. Float, explode or sink: postmortem fate of lung-breathing marine vertebrates. Palaeobiodiversity and Palaeoenvironments 92, 67–81. https://doi.org/10.1007/s12549-011-0067-z.

Renesto, S., Dal Sasso, C., Fogliazza, F., Ragni, C., 2020. New findings reveal that the Middle Triassic ichthyosaur *Mixosaurus cornalianus* is the oldest amniote with a dorsal fin. Acta Palaeontologica Polonica 65 (3), 511–522. https://doi.org/10.4202/app.00731.2020.

Rossi, V., Bernardi, M., Fornasiero, M., Nestola, F., Unitt, R., Castelli, S., Kustatscher, E., 2024. Forged soft tissues revealed in the oldest fossil reptile from the early Permian of the Alps. Palaeontology 67 (1), e12690. https://doi.org/10.1111/pala.12690.

Schäfer, W., 1972. Ecology and palaeoecology of marine environments. University of Chicago Press.

Schmitt, J., Flemming, H.C., 1998. FTIR-spectroscopy in microbial and material analysis. International Biodeterioration & Biodegradation 41 (1), 1–11. https://doi.org/10.1016/s0964-8305(98)80002-4.

Schroeder, A.B., Dobson, E.T., Rueden, C.T., Tomancak, P., Jug, F., Eliceiri, K.W., 2021. The ImageJ ecosystem: Open-source software for image visualization, processing, and analysis. Protein Science 30 (1), 234–249. https://doi.org/10.1002/pro.3993.

Schultze, H.P., Stöhr, D., 1996. *Vinctifer* (Pisces, Aspidorhynchidae) aus der unterkreide (oberes Aptium) von Kolumbien. Neues Jahrbuch für Geologie und Paläontologie - Abhandlungen 199 (3), 395–415. https://doi.org/10.1127/njgpa/199/1996/395.

Schweitzer, M.H., 2011. Soft tissue preservation in terrestrial Mesozoic vertebrates. Annual Review of Earth and Planetary Sciences 39 (1), 187–216. https://doi.org/10.1146/annurev-earth-040610-133502.

Schweitzer, M.H., Zheng, W., Cleland, T.P., Bern, M., 2013. Molecular analyses of dinosaur osteocytes support the presence of endogenous molecules. Bone 52 (1), 414–423. https://doi.org/10.1016/j.bone.2012.10.010.

Schweitzer, M.H., Zheng, W., Cleland, T., Goodwin, M.B., Boatman, E., Theil, E., Marcus, M.A., Fakra, S.C., 2014. A role for iron and oxygen chemistry in preserving soft tissues, cells and molecules from deep time. Proceedings of the Royal Society B: Biological Sciences 281, 20132741. https://doi.org/10.1098/rspb.2013.2741.

Schweitzer, M.H., Schroeter, E.R., Cleland, T.P., Zheng, W., 2019. Paleoproteomics of Mesozoic dinosaurs and other Mesozoic fossils. Proteomics 19 (16), 1800251. https://doi.org/10.1002/pmic.201800251.

Scotese, C.R., 2021. An atlas of Phanerozoic paleogeographic maps: the seas come in and the seas go out. Annual Review of Earth and Planetary Sciences 49 (1), 679–728. https://doi.org/10.1146/annurev-earth-081320-064052.

Seilacher, A., Reif, W.E., Westphal, F., 1985. Sedimentological, ecological and temporal patterns of fossil Lagerstätten. Philosophical Transactions of the Royal Society of London B Biological Sciences 311 (1148), 5–24. https://doi.org/10.1098/rstb.1985.0134.

Senter, P.J., 2022. Cells and soft tissues in fossil bone: A review of preservation mechanisms, with corrections of misconceptions. Palaeontologia Electronica 25 (3), a34. https://doi.org/10.26879/1248.

Signore, M., Bucci, E., Pede, C., Barbera, C., 2005. A new ichthyodectid fish from the Lower Cretaceous of Pietraroja (Southern Italy). PalArch 5, 25–29.

Sinha, S., Muscente, A.D., Schiffbauer, J.D., Williams, M., Schweigert, G., Martindale, R.C., 2021. Global controls on phosphatization of fossils during the Toarcian oceanic anoxic event. Scientific Reports 11, 24087. https://doi.org/10.1038/s41598-021-03482-7.

Smithwick, F., 2019. A taphonomic and palaeoecological approach to the study of palaeocolour. Doctoral dissertation, University of Bristol.

Smithwick, F.M., Mayr, G., Saitta, E.T., Benton, M.J., Vinther, J., 2017. On the purported presence of fossilized collagen fibres in an ichthyosaur and a theropod dinosaur. Palaeontology 60 (3), 409–422. https://doi.org/10.1111/pala.12292.

Thermo Fisher Scientific. Electron beam damage in scanning electron microscopes: An overview of the damage caused to samples by electron beams. n.d. https://www.thermofisher.com/us/en/home/materials-science/learning-center/applications/sample-degradation-scanning-electron-microscope-sem.html. (Accessed 16 June 2025).

Tuinstra, F., Koenig, J.L., 1970. Raman spectrum of graphite. The Journal of Chemical Physics 53 (3), 1126–1130. https://doi.org/10.1063/1.1674108.

Ullmann, P.V., Pandya, S.H., Nellermoe, R., 2019. Patterns of soft tissue and cellular preservation in relation to fossil bone tissue structure and overburden depth at the Standing Rock Hadrosaur Site, Maastrichtian Hell Creek Formation, South Dakota, USA. Cretaceous Research 99, 1–13. https://doi.org/10.1016/j.cretres.2019.02.012.

Vistoli, G., De Maddis, D., Cipak, A., Zarkovic, N., Carini, M., Aldini, G., 2013. Advanced glycoxidation and lipoxidation end products (AGEs and ALEs): an overview of their mechanisms of formation. Free Radical Research 47 (Suppl. 1), 3–27. https://doi.org/10.3109/10715762.2013.815348.

Welles, S.P., 1962. A new species of elasmosaur from the Aptian of Colombia and a review of the Cretaceous plesiosaurs, 44. University of California Publications in the Geological Sciences, pp. 1–96.

Wiemann, J., Briggs, D.E., 2022. Raman spectroscopy is a powerful tool in molecular paleobiology: An analytical response to Alleon et al. BioEssays 44 (2), 2100070. https://doi.org/10.1002/bies.202100070, 10.1002/bies.202000295.

Wiemann, J., Fabbri, M., Yang, T.R., Stein, K., Sander, P.M., Norell, M.A., Briggs, D.E., 2018. Fossilization transforms vertebrate hard tissue proteins into N-heterocyclic polymers. Nature Communications 9 (1), 4741. https://doi.org/10.1038/s41467-018-07013-3.

Xu, X., Zhou, Z., Wang, Y., Wang, M., 2020. Study on the Jehol Biota: recent advances and future prospects. Science China Earth Sciences 63, 757–773. https://doi.org/10.1007/s11430-019-9509-3.

Yang, Z., Jiang, B., Xu, J., McNamara, M.E., 2024. Cellular structure of dinosaur scales reveals retention of reptile-type skin during the evolutionary transition to feathers. Nature Communications 15 (1), 4063. https://doi.org/10.1038/s41467-024-48400-3.